Electronic States of Porphycenes

Jacek Waluk,[1a,b] Monika Müller,[1c] Petra Swiderek,[1c] Matthias Köcher,[1c] Emanuel Vogel,[1c] Georg Hohlneicher,*[,1c] and Josef Michl*[,1a]

Contribution from the Center for Structure and Reactivity, Department of Chemistry and Biochemistry, The University of Texas at Austin, Austin, Texas 78712-1167, and Institut für Organische Chemie der Universität Köln, Greinstrasse 4, D-5000, FRG.
Received October 26, 1990

Abstract: Polarized UV–visible absorption, emission, and magnetic circular dichroism of a series of porphycenes are reported and interpreted in terms of the classical perimeter model as well as semiempirical CNDO/S, INDO/S, and PPP calculations. Differences relative to porphyrins follow readily from their different topology. Two results are particularly striking: (i) unlike the soft MCD chromophores, porphyrins, the porphycenes are negative-hard chromophores and provide a clear example of the competition between the μ^+ contributions and the μ^- contributions to the B terms of the Soret bands and (ii) fluorescence polarization results for free-base porphycene suggest the existence of a fast intramolecular proton-transfer process in the first singlet excited state, which calls for a closer examination by time-resolved methods.

Due to a multitude of intriguing physical, chemical, and biological properties, the porphyrins and their metal complexes stir interdisciplinary interest. Used by nature in the most important process of photosynthesis and in solving transport and other problems in living systems, these tetrapyrrolic macrocycles have been very fittingly described as "pigments of life".[2] In addition, porphyrins and their nonnatural congeners, the phthalocyanins, play an essential role as components of devices in the rapidly growing field of organic materials with unusual properties.[3] As regards their well-known application in medicine, much of the current research activity focuses on the utilization of these dyes and pigments in the detection and photodynamic therapy of tumors.[4]

The fact that the biological significance of the porphyrins arises from their properties as chromophores has captured the imagination of spectroscopists from the early days on, and their molecular design and structural variability have made them particularly attractive. The general structure of the underlying chromophores is usually easily understood in terms of simple models. Finer details, however, that often lead to considerable differences between otherwise fairly similar systems, are frequently difficult to grasp. As a result, the literature contains hundreds of publications that deal with the spectroscopy of compounds of this kind, mostly with porphyrins and phthalocyanins; for survey articles, see, for example, ref 5.

With the synthesis of porphycene (**1**),[6] a tetrapyrrolic structural isomer of porphyrin (**2**), a new type of porphyrinoid system became available a few years ago. Similar to porphyrins, porphycenes are stable aromatic pigments that are capable of forming metal

Chart I

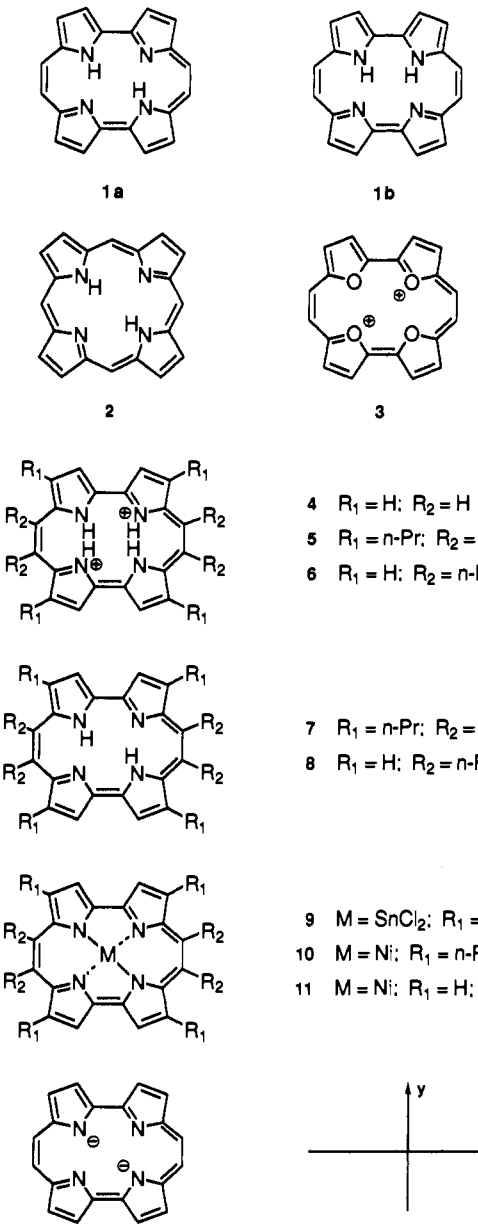

(1) (a) The University of Texas at Austin. Present address: Department of Chemistry and Biochemistry, University of Colorado, Boulder, CO 80309-0215. (b) Permanent address: Institute of Physical Chemistry, Polish Academy of Sciences, 01-224 Warsaw, Poland. (c) University of Cologne.

(2) Battersby, A. R.; Fookes, C. J. R.; Matcham, G. W. J.; McDonald, E. *Nature (London)* **1980**, *285*, 17. Kräutler, B. *Chimia* **1987**, *41*, 277.

(3) Organic metals: Hanack, M. *Chimia* **1983**, *37*, 238. Marks, T. J. *Science (Washington, D.C)* **1985**, *227*, 881. Collman, J. P.; McDevitt, J. T.; Yee, G. T.; Leitner, C. R.; McCullough, L. G.; Little, W. A.; Torrance, J. B. *Proc. Natl. Acad. Sci. U.S.A.* **1986**, *83*, 4581. Photosynthetic models: Weiser, J.; Staab, H. A. *Angew. Chem., Int. Ed. Engl.* **1984**, *23*, 623. Wasielewski, M. R.; Niemczyk, M. P.; Svec, W. A.; Pewitt, E. B. *J. Am. Chem. Soc.* **1985**, *107*, 5562. Effenberger, F.; Schlosser, H.; Bäuerle, P.; Maier, S.; Port, H.; Wolf, H. C. *Angew. Chem., Int. Ed. Engl.* **1988**, *27*, 281. Gust, D.; Moore, T. A. *Science (Washington, D.C.)* **1989**, *244*, 35. Gust, D.; Moore, T. A.; Lee, S.-J.; Bittersmann, E.; Luttrull, D. K.; Rehms, A. A.; DeGraciano, J. M.; Ma, X. C.; Gao, F.; Belford, R. F.; Trier, T. T. *Science (Washington, D.C.)* **1990**, *248*, 199. Liquid crystals: Sirlin, C.; Bosio, L.; Simon, J. *J. Chem. Soc., Chem. Commun.* **1987**, 379.

(4) Franck, B. *Angew. Chem., Int. Ed. Engl.* **1982**, *21*, 343. Kessel, D., Dougherty, T., Eds. *Porphyrin Photosensitization, Advances in Experimental Medicine and Biology 160*; Plenum: New York, 1983. Andreoni, A., Cubeddo, R., Eds. *Porphyrins in Tumor Phototherapy*; Plenum: New York, 1984.

(5) (a) Gouterman, M. In *The Porphyrins*; Dolphin, D., Ed.; Academic Press: New York, 1978; Vol. III, p 1. (b) Goldbeck, R. A. *Acc. Chem. Res.* **1988**, *21*, 95.

(6) (a) Vogel, E.; Köcher, M.; Schmickler, H.; Lex, J. *Angew. Chem., Int. Ed. Engl.* **1986**, *25*, 257. (b) Köcher, M. Ph.D. Dissertation, University of Cologne, Germany, 1989.

0002-7863/91/1513-5511$02.50/0

complexes (metalloporphycenes) with many metal ions, although their coordination cavity is noticeably smaller than that of the porphyrins. As a general method of synthesis of porphycenes has since been developed,[7] allowing these compounds to be made in great structural variety, a physical and chemical comparison between porphycenes and porphyrins suggests itself.

The initial exploration of **1** has already shown that the electronic spectra[6] of the two types of tetrapyrrolic macrocycles exhibit both striking similarities and striking differences.[8] NMR studies[8b] have shown that both the trans (**1a**) and the cis (**1b**) tautomers are present to a significant degree in the ground state. It is the purpose of the present study to characterize the polarized absorption and emission as well as magnetic circular dichroism (MCD) of a series of porphycenes in the UV and visible regions (**1** and **3–12** in Chart I) and to establish that the similarities as well as the differences with respect to porphyrins can be understood not only on the basis of CNDO/S[9] and INDO/S[10] calculations, but also in terms of the simple and general perimeter model,[11-14] applicable to all π-electron systems derivable from a $(4N+2)$-electron [n]annulene perimeter. Like other such systems derived from a charged perimeter ($n \neq 4N+2$), porphycenes exhibit two nearly degenerate low-energy transitions (L_1 and L_2 in the standard perimeter model notation) and two nearly degenerate transitions at higher energy (B_1 and B_2). In the case of porphyrins, it is customary to refer to the two L bands, located near 600 nm, as Q_x and Q_y, and to the two usually strongly overlapping B bands, located near 400 nm, as the Soret band. Because of the similarity between the spectra of porphycenes and porphyrins, we shall also use the labels Q and Soret, respectively, to refer to the L and B transitions of porphycenes, but it is important to keep in mind that these are merely particular cases of the more generally encountered L and B transitions.

Experimental Section and Calculations

Materials. Preparation of pure samples of **1** and **3–11** has been described elsewhere.[6,7] Freshly distilled 2-methyltetrahydrofuran (2-MTHF) was dried by passing over a column filled with ICN Alumina B Super I. Orthophosphoric acid (85%, chemically pure, Riedel-de Haen) was used as purchased. Methylene chloride (Malinckrodt, spectral grade), H_2SO_4 (Alfa, ultra pure), $HClO_4$ (Alfa, doubly distilled), and *n*-hexane (Baker, spectral purity) were used as received. Porphycene dianion was prepared in a mixture of tetrahydrofuran (distilled over sodium) and potassium *tert*-butoxide (Aldrich).

Spectroscopy. At Cologne, absorption spectra were measured with a Perkin-Elmer 559 UV/vis spectrophotometer with a commercial low-temperature adaptor. Room temperature measurements were done in 1-cm, and low-temperature measurements (~77 K if not stated otherwise) in 5-mm Suprasil cells. Concentrations have not been corrected for solvent contraction. Polarized fluorescence and excitation spectra were measured with a homemade instrument described in ref 15. At Austin, absorption spectra were measured in 1-cm cells with a Varian 2300 spectrophotometer. MCD spectra were measured at room temperature with a JASCO J-600 spectropolarimeter equipped with a 15-kG electromagnet, wavelength calibrated with a holmium oxide filter and scale calibrated with the CD of *d*-camphorsulfonic acid and the MCD of naphthalene as described in ref 16. Polarized fluorescence and excitation spectra were measured on a homemade instrument described earlier.[17]

Linear dichroism (LD) of **1**, **8**, **10**, and **11** embedded in stretched polyethylene sheets was measured partially at Austin and partially at Cologne with the techniques described in ref 17. The identification of the higher dichroic ratio with the physically longer axis is based on the empirical relationships discussed in ref 18.

Calculations. As far as possible, input geometries were obtained from X-ray data. The CNDO/S[9] method was used to calculate transition energies and dipole strengths, using 200 energy-selected singly and doubly excited configurations.[19] Electron repulsion integrals were approximated by the Pariser formula.[20] All other parameters were taken from the final parameterization of the CNDO/S method.[21] The ground-state depression that results from the inclusion of doubly excited configurations was not neglected in calculating excitation energies as it was in our earlier work.[22] Neglect of the ground-state depression would lead to much too

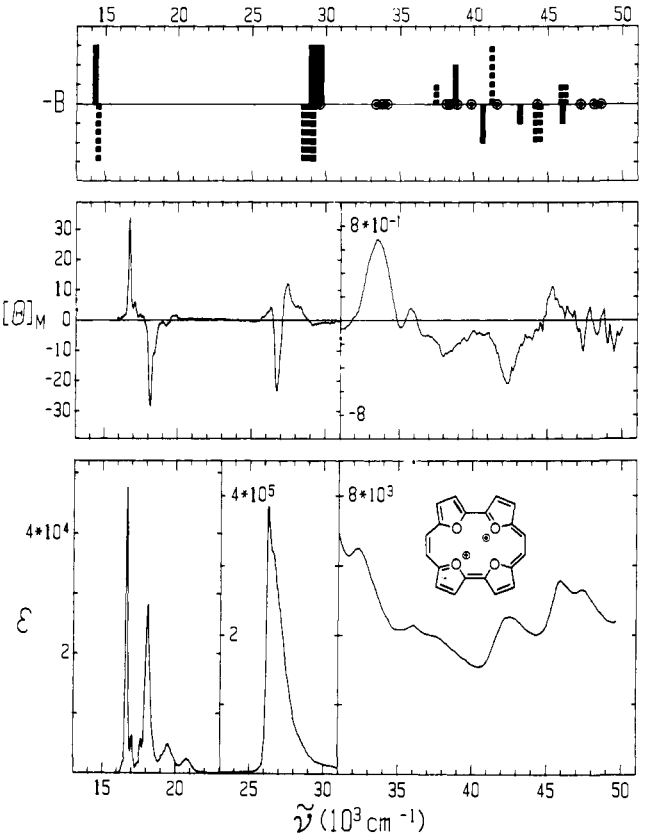

Figure 1. Tetraoxaporphycene dication (**3**): top, the INDO/S result, the height of the bars represents the magnitude and sign of the calculated *B* term, the width of the bars reflects the calculated dipole strength, full bars refer to *x*-polarized transitions, dashed bars to *y*-polarized ones, circles represent forbidden transitions; center, MCD spectrum; bottom, room temperature absorption spectrum; solvent, H_2SO_4.

(7) (a) Vogel, E.; Balci, M.; Pramod, K.; Koch, P.; Lex, J.; Ermer, O. *Angew. Chem., Int. Ed. Engl.* **1987**, *26*, 928. (b) Vogel, E.; Köcher, M.; Lex, J.; Ermer, O. *Isr. J. Chem.* **1989**, *29*, 257. (c) Vogel, E. *Pure Appl. Chem.* **1990**, *62*, 557.

(8) A similar situation is obtained with most of the other spectra of porphycenes investigated so far. (a) Photophysics: Aramendia, P. F.; Redmond, R. W.; Nonell, S.; Schuster, W.; Braslawsky, S. E.; Schaffner, K.; Vogel, E. *Photochem. Photobiol.* **1986**, *44*, 555. (b) ^{15}N-CPMAS NMR: Wehrle, B.; Limbach, H.-H.; Köcher, M.; Ermer, O.; Vogel, E. *Angew. Chem., Int. Ed. Engl.* **1987**, *26*, 934. (c) ESR and ENDOR: Schlüpmann, J.; Huber, M.; Toporowicz, M.; Köcher, M.; Vogel, E.; Levanon, H.; Möbius, K. *J. Am. Chem. Soc.* **1988**, *110*, 8566. Renner, M. W.; Forman, A.; Wu, W.; Chang, C. K.; Fajer, J. *Ibid.* **1989**, *111*, 8618. (d) Time-resolved ESR: Ofir, H.; Regev, A.; Levanon, H.; Vogel, E.; Köcher, M.; Balci, M. *J. Phys. Chem.* **1987**, *91*, 2686.

(9) Del Bene, J.; Jaffé, H. H. *J. Chem. Phys.* **1968**, *48*, 1807, 4050. *Ibid.* **1968**, *49*, 1221. *Ibid.* **1969**, *50*, 1126.

(10) Ridley, J.; Zerner, M. C. *Theor. Chim. Acta* **1973**, *32*, 111. *Ibid.* **1976**, *42*, 223.

(11) Platt, J. R. *J. Chem. Phys.* **1949**, *17*, 484.

(12) Moffitt, W. *J. Chem. Phys.* **1954**, *22*, 320, 1820.

(13) Gouterman, M. *J. Mol. Spectrosc.* **1961**, *6*, 138.

(14) (a) Michl, J. *J. Am. Chem. Soc.* **1978**, *100*, 6801. (b) Michl, J. *J. Am. Chem. Soc.* **1978**, *100*, 6812. (c) Michl, J. *J. Am. Chem. Soc.* **1978**, *100*, 6819.

(15) Frölich, W. Ph.D. Thesis, University of Cologne, Germany, 1979.

(16) Böttcher, A.; Raabe, G.; Michl, J. *J. Org. Chem.* **1985**, *50*, 5050.

(17) Kolc, J.; Michl, J.; Vogel, E. *J. Am. Chem. Soc.* **1976**, *98*, 3935.

(18) (a) Thulstrup, E. W.; Michl, J. *J. Am. Chem. Soc.* **1982**, *104*, 5594. (b) Michl, J.; Thulstrup, E. W. *Spectroscopy with Polarized Light. Solute Alignment by Photoselection, in Liquid Crystals, Polymers, and Membranes*; VCH Publishers: Deerfield Beach, FL, 1986; see also references therein.

(19) Dick, B.; Hohlneicher, G. *Theor. Chim. Acta* **1979**, *53*, 221.

(20) Pariser, R. *J. Chem. Phys.* **1953**, *21*, 568.

(21) Ellis, R. L.; Kuehnlenz, G.; Jaffé, H. H. *Theor. Chim. Acta* **1972**, *26*, 131.

(22) (a) Boersch-Pulm, B.; Demmer, M.; Murthy, G. S.; Lex, J.; Schieb, Th.; Vogel, E.; Hohlneicher, G.; Michl, J. *J. Phys. Chem.* **1987**, *91*, 1382. (b) Frölich, W.; Dewey, H. J.; Deger, H.; Dick, B.; Klingensmith, K. A.; Püttmann, W.; Vogel, E.; Hohlneicher, G.; Michl, J. *J. Am. Chem. Soc.* **1983**, *105*, 6211. (c) Dewey, H. J.; Deger, H.; Frölich, W.; Dick, B.; Klingensmith, K. A.; Hohlneicher, G.; Vogel, E.; Michl, J. *J. Am. Chem. Soc.* **1980**, *102*, 6412.

Table I. Experimental Results for the Low-Energy Part of Electronic Spectra of Porphycenes[a]

compd	solvent		L_1 (Q_1)	L_2 (Q_2)	X	B_1	Soret	B_2	Y	ΔL	ΔB	$D(L)/D(B)$[b]	$\bar{\nu}(Q_1)$[c]	$\bar{\nu}(Q_2)$[c]
3	H_2SO_4	*E*	16700	18100		26200		(26700)		1400	500			
		B	−16.6	19.1		9.5		−11.9						
	H_3PO_4	*E*	16690	18120			26000			1430			340	190
		f	0.033	0.053			1.95					0.066		
4	$HClO_4$	*E*	16100	17200		24900		26600	29500	1100	1700			
		B	−32.5	49.6		2.5		−6.8	6.0					
	H_3PO_4	*E*	16010	17180		24850		26540		1170	1690		330	320
		f	0.048	0.11		0.29		0.88				0.21		
5	H_3PO_4	*E*	15980	17120		24290		25990		1140	1700			
		f	0.076	0.11		0.50		1.12				0.16		340
6	H_3PO_4	*E*	14990	16250		23130		24950	30000	1260	1820		280	330
		f	0.085	0.11		0.26		1.18				0.21		
1	CH_3CN	*E*	16000	16900	23500	27100		28100	30000	900	1000		160	160
		B	−48.0	65.1	1.2		−19.6		6.2					
	2-MTHF	*E*	15800	16700	25000	27000		28000		900	1000		170	170
		f	0.12	0.16	0.05		1.32					0.35		
7	CH_3CN	*E*	15800	16700	23000	26300		27200	30000	900	900			
		B	−41.3	53.5			−18.6		4.9					
	2-MTHF	*E*	15740	16620	24300	26300		27130		880	800		180	160
		f	0.13	0.20			1.50					0.36		
8	CH_3CN	*E*	15200	15900	23000	26000		27000	29000	700	1000			
		B	−44.2	66.1			−21.3		8.0					
	2-MTHF	*E*	15130	15640		25800		26720		510	900		260	
		f	0.36				1.39					0.41		
9	2-MTHF	*E*	15920	16420	23600	25030		25590		500	560			
		f	0.26	0.25			1.49					0.53		
10	*n*-hexane	*E*	16200	16500	23500		25900		30000	300				
		B	−62.7	81.1			−18.8		1.3					
	2-MTHF	*E*	16330	16610	23800		25890			280			260	
		f	0.33				1.09					0.48		
11	*n*-hexane	*E*	15500				25400		28000					
		B	−32.7	42.3			−13.3		2.5					
	2-MTHF	*E*	15510		23000		25480							
		f	0.35				1.15					0.50		
12	THF	*E*	15000	15300	23000		26600		28500	300				
		B	−54.9	68.7	2.1		−15.1		6.5					
		f	0.33				1.51							

[a] Key: *E*, transition energy (cm^{-1}). *B*, *B* term ($D^2 \times \mu_B/cm^{-1}$): ΔL, L_1–L_2 separation: ΔB, B_1–B_2 separation. [b] Obtained from the ratio of oscillator strengths by multiplying by the ratio of the estimated mean frequencies of Q and Soret transitions. [c] Frequencies of low-energy vibrations that accompany the origins of the Q bands (see text).

low energies for the L transitions. Consequently, the excitation energies for the higher transitions are overestimated by 3000–6000 cm^{-1}. This overestimation results from an unbalanced influence of the neglected triply and quadruply excited configurations on the low-lying excited states.

The INDO/S method and the PPP method were used to calculate transition energies, dipole strengths, and *B* terms, including up to 200 singly excited configurations. In the PPP calculations, a value of −0.15 was used for the ratio of the resonance integrals between nearest and next-nearest neighbors.[14]

Results

General Results (Table I). The absorption spectra resemble those of porphyrins with a Q-band region between 15000 and 23000 cm^{-1}, and a Soret-band region between 25000 and 30000 cm^{-1}. The Q-band region often exhibits a well-resolved vibrational structure, as in most porphyrins, but has higher intensity, and the 0–0 transitions are much more pronounced. In spite of the similarity of the transition energies, this leads to a completely different appearance of the visible part of the absorption spectra of the two classes of compounds. As in porphyrins, the Q as well as the Soret transition pairs are each nearly degenerate. In contrast to the MCD spectra of most porphyrins, the Q_1 band of porphycenes always has a negative and the Q_2 band a positive *B* term (i.e., appears as positive and negative peaks in the MCD spectrum, respectively). The *B* terms of the Soret bands are weak and negative; only in the tetraoxa compound **3** and in the dication **4** is the *B* term of the lower Soret band positive. For the free bases and the salts **1** and **7–12**, an additional weak band (X) is observed between the Q and Soret regions. Its *B* term is very small but always positive. At the high-energy side of the Soret bands, an additional transition (Y) is found that also has a positive *B* term. An analogous transition was observed in a number of porphyrin systems.[23] No further prominent absorption bands are observed up to 50000 cm^{-1}. The MCD spectra, however, clearly reveal quite a number of different transitions in this energy range.

Tetraoxaporphycene Dication (3) (Figure 1). From the temperature dependence of the absorption spectrum (Figure 2), it is obvious that the shoulder observed at the low-energy side of the 16690 cm^{-1} maximum is a hot band caused by a vibration of about 330 cm^{-1}. A similar frequency also appears in the fluorescence spectrum. The maximum at 16700 cm^{-1} is undoubtedly the 0–0 transition of the first Q band. This band corresponds to a sharp maximum in the MCD spectrum. On the high-energy side of the 0–0 peak of Q_1, a 340 cm^{-1} vibration is clearly discernible.

The second intense low-energy band at 18100 cm^{-1} coincides with a sharp minimum in the MCD curve. We assign this peak as the 0–0 transition of the second Q band. This corresponds to a split of 1400 cm^{-1} between the two Q-band origins. Shoulders on the high-energy side of this band point to a vibration of about 190 cm^{-1}. By integrating from 16000 to 17750 cm^{-1} and from 17750 to 22000 cm^{-1}, we obtain oscillator strengths of 0.033 for Q_1 and 0.053 for Q_2. Due to the unresolved overlap of the two bands, these values provide a lower limit for Q_1 and an upper limit for Q_2. The overlap between Q_1 and Q_2 also leads to some cancellation in the MCD bands, with the result that the true *B* terms

(23) (a) Djerassi, C.; Lu, Y.; Waleh, A.; Shu, A. Y. L.; Goldbeck, R. A.; Kehres, L. A.; Crandell, C. W.; Wee, A. G. H.; Knierzinger, A.; Gaete-Holmes, R.; Loew, G. H.; Clezy, P. S.; Bunnenberg, E. *J. Am. Chem. Soc.* **1984**, *106*, 4241. (b) Goldbeck, R. A.; Tolf, B.-R.; Wee, A. G. H.; Shu, A. Y. L.; Records, R.; Bunnenberg, E.; Djerassi, C. *J. Am. Chem. Soc.* **1986**, *108*, 6449.

Table II. Experimental Results for the High-Energy Part of Electronic Spectra of Porphycenes[a]

3	*E*	32 300	sh			36 000	sh	42 500		45 900	47 400
	ε	6500				4200		4500		5600	5300
	MCD		33 400 (+)	35 000 (-)		35 900 (+)	38 000 (-)	42 200 (-)		45 200 (+)	
4	*E*		33 600			sh		sh	42 300		
	ε		8700			5000		4100	5000		
	MCD	32 500 (-)	34 200 (+)			36 100 (-)		41 000 (-)			
5	*E*	31 400						41 000 sh		45 000	
	ε	14 000						5000		8900	
6	*E*		33 000				39 000		43 000		
	ε		8000				6000		8500		
1	*E*						39 000 sh	42 200			50 000
	ε						5700	8500			12 000
	MCD					37 000 (+)		41 800 (-)			
7	*E*						39 000 sh	41 800	sh		50 000
	ε						9100	12 500			20 000
	MCD					3u 100 (+)		40 600 (-)	40 600 (-)		
8	*E*							40 800	sh		48 500
	ε							15 000			20 000
	MCD							40 200 (-)	42 400 (+)	46 500 (-)	
9	*E*	32 700									
	ε	29 200									
10	*E*		34 000		37 900						49 000
	ε		15 000		30 000						58 000
	MCD			36 200 (-)	37 300 (-)	38 300 (+)		40 200 (-)	42 000 (+)		
11	*E*		34 000	35 900	37 500 sh			39 500	41 200 sh		49 000
	ε		15 000	26 000	24 000			21 000	19 000		46 000
	MCD			35 900 (-)	37 100 (-)	38 100 (+)		39 500 (-)	41 200 (+)		
				37 200			38 000 sh				
				3000			22 400				

[a] Key: *E*, transition energy (cm^{-1}); sh, shoulder; ε, molar decadic extinction coefficient; MCD, position (sign) of peaks (cm^{-1}).

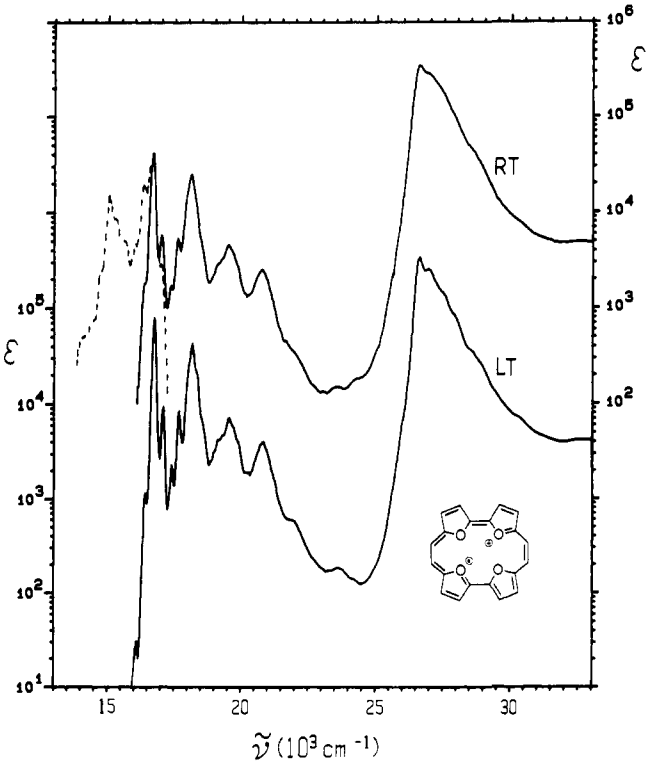

Figure 2. Absorption and emission spectra of the tetraoxaporphycene dication (**3**) in H_3PO_4: RT, room temperature (scale on the right); LT, ~200 K (scale on the left).

may be substantially larger than those obtained from the observed band areas.

The two Soret bands overlap even more strongly. A minimum at 26 700 cm^{-1} in the MCD curve does not coincide with the absorption maximum at 26 200 cm^{-1}, and there is a weak third band in the MCD at the low-energy side, complicating the assignment. We attribute the strong negative MCD peak to the lower and the strong positive MCD peak to the higher Soret band but admit that explicit consideration of vibronic interactions may be necessary for detailed understanding. The split between the two bands can hardly exceed 500 cm^{-1}. Due to their strong overlap, it is not possible to derive a reasonable estimate of their intensity ratio. In the MCD spectrum, the overlap of the two bands must lead to a cancellation of positive and negative contributions, producing a feature sometimes referred to as a "pseudo-*A* term". The *B* terms are definitely larger in absolute magnitude than shown in Table I, obtained by separate integration of the negative and positive parts of the spectrum.

At energies between 30 000 and 50 000 cm^{-1}, the absorption spectrum shows only some weak bands of medium intensity. From the MCD curve, it is obvious that this part of the spectrum results from a number of different transitions (Table II).

N-Protonated Porphycene Dications 4–6. Protonation of the two pyridine-type nitrogens in **1** does not change the overall appearance of the electronic spectrum, in spite of the fact that protonated porphycenes are certainly no longer strictly planar. Compared to that in the metal salts discussed below, the split between the two Q and the two Soret bands in **4–6** is somewhat larger. The intensity ratio of the Q to the Soret bands is larger than in **3** and smaller than in the metal complexes discussed below (Table I).

The first maximum at 16 000 cm^{-1} in the absorption spectrum of **4** (Figure 3) again coincides with a very sharp maximum in the MCD curve. From the fluorescence spectrum, it is quite obvious that the Q_1 band must have a considerable overlap with the Q_2 band, which has its origin at about 17 200 cm^{-1}. The oscillator strengths that we obtain from the integrated band areas therefore provide only a lower limit for Q_1 and an upper limit for Q_2. The same is surely true for the two Soret bands. The vibrational structure observed in the Q-band region becomes somewhat more pronounced when the sample is cooled down to about 200 K (methanol/dry ice). The low-energy vibrations discernible at that temperature are on the order of 320 cm^{-1} for both Q bands.

There certainly again is some cancellation of positive and negative *B* terms, both in the Q and in the Soret regions, due to the strong overlap of two oppositely signed bands. The *B* term sign sequence for the four low-energy bands is −, +, +, −. The minimum at about 29 500 cm^{-1} (Y) is somewhat more pronounced than in **3**. At higher energies, the absorption spectrum again shows only medium-intense bands with little structure. Considering the variations seen in the MCD curve (Figure 3 and Table II), these bands must again result from a number of different transitions.

n-Propyl substituents at the heterocyclic rings (**5**) have little influence on the absorption spectrum (Figure 4, Tables I and II). There are slight changes in the relative intensities, but the separation between the two Q and the two Soret bands is nearly unchanged. The *n*-propyl substituents have a somewhat larger

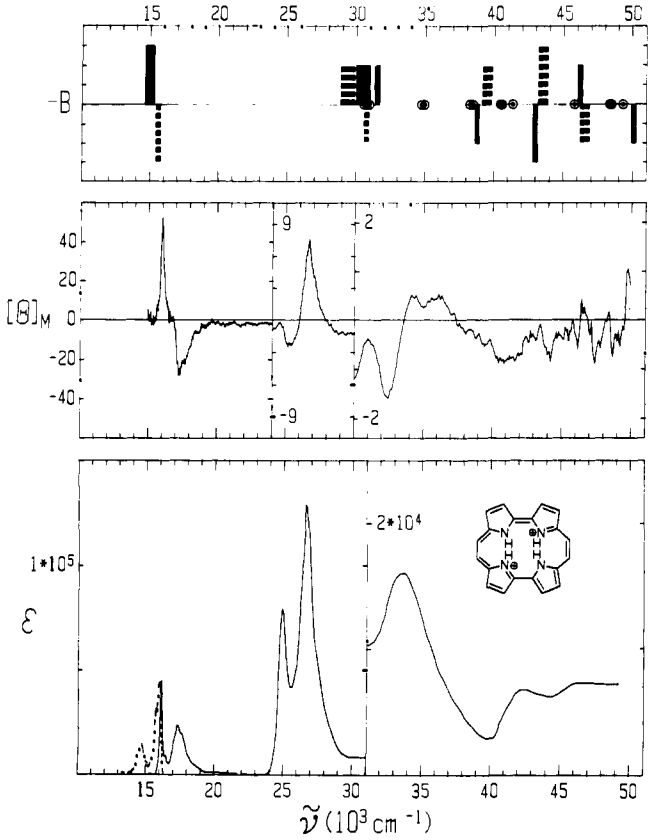

Figure 3. Porphycene dication (**4**). See caption to Figure 1. The dashed line is room temperature fluorescence: solvent, $HClO_4$.

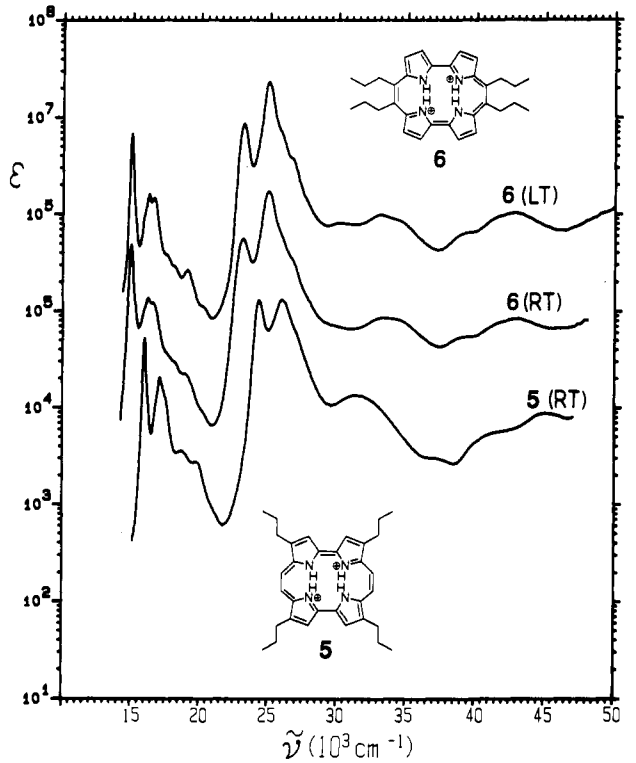

Figure 4. *n*-Propyl-substituted porphycene dications **5** and **6**: RT, room temperature; LT, ~200 K. The scale applies to the bottom curve; the others have been displaced by one or two log units.

influence when located at the ethylene bridges (**6**, Figure 4, Tables I and II). Both band systems are shifted by about 1000 cm^{-1} to lower energies. This low-energy shift of the Soret band reveals a shallow maximum around 30 000 cm^{-1}. The splitting between the Q and the Soret bands in **6** is slightly larger than in **4** and **5** (Table I). The vibrational structure in the Q band becomes

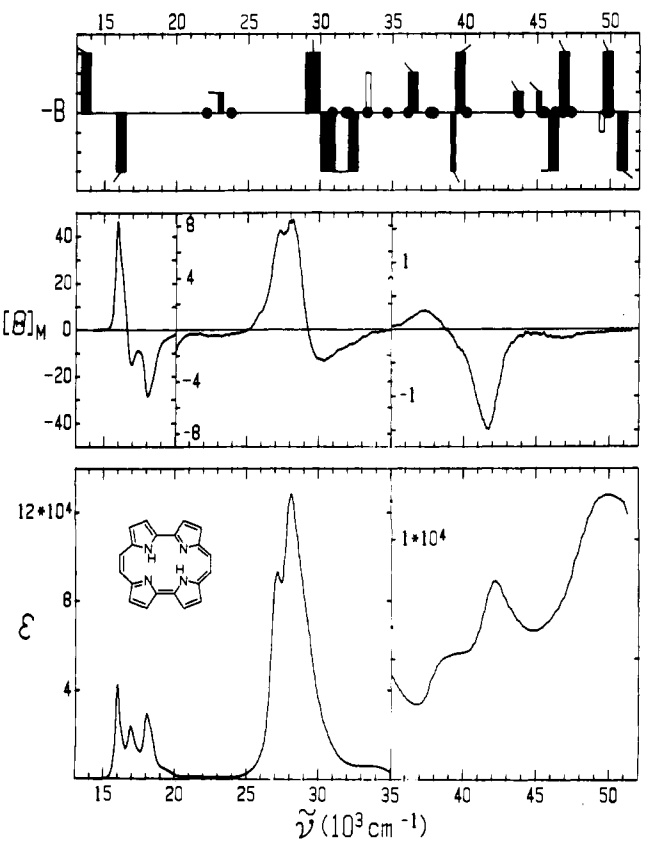

Figure 5. Porphycene free base (**1**). See caption to Figure 1. The flags on the bars in the upper part represent the orientation of the transition dipole moments relative to the formula shown. Open bars refer to *z*-polarized $n\pi^*$ transitions: solvent, CH_3CN.

somewhat more pronounced when the sample is cooled to 200 K. Low-energy vibrations of 280 and 330 cm^{-1} can be detected for Q_1 and Q_2, respectively. There is also some indication of a 700–800 cm^{-1} vibration in the upper Soret band.

Porphycene Free Base (1). The first absorption maximum at 16 000 cm^{-1} (Figure 5) again corresponds to a positive peak in the MCD curve. The second absorption maximum at 16 900 cm^{-1} coincides with a negative MCD peak and is assigned to the onset of Q_2. The third absorption maximum at 18 100 cm^{-1} is considerably more intense than in **3**. It appears in the substituted free bases, too, and moves with the onset of Q_2. We therefore assign it as a vibrational band (1200 cm^{-1}) of Q_2. A vibration of similar frequency is seen in the metal salts. The intensity of the Q bands relative to the Soret bands is higher than in **3–6**. At the onset of the Soret band region around 25 000 cm^{-1}, we observe a weak band (X) that was not seen in **3** and in the N-protonated compounds **4–6**. This transition is probably responsible for the broad negative peak in the MCD curve between 22 000 and 25 000 cm^{-1}. The Soret-band region itself shows a pattern similar to that observed in the protonated forms **4–6**, with a split of about 1000 cm^{-1}. However, the MCD curve is now positive for both bands so that both transitions have negative *B* terms. Only at the high-energy side of the Soret bands (around 30 000 cm^{-1}) do we find a shallow minimum in the MCD curve, which we attribute to the transition labeled Y, as in all the other compounds investigated.

At low temperature, considerable vibrational structure is revealed in the Q-band region (Figure 6). A soft mode of 160 ± 10 cm^{-1} couples to the origins of Q_1 and Q_2. A mode of similar frequency is seen in fluorescence, too (Figure 6). No indication of fluorescence from Q_2 was found. We were therefore surprised to observe a nearly completely depolarized fluorescence excitation spectrum. This measurement was independently done in EPA at Austin and in 2-MTHF at Cologne. In both cases, the degree of polarization (*P*) lies between 0 and 0.15 in the whole spectral range. It is definitely different from zero at most wavelengths,

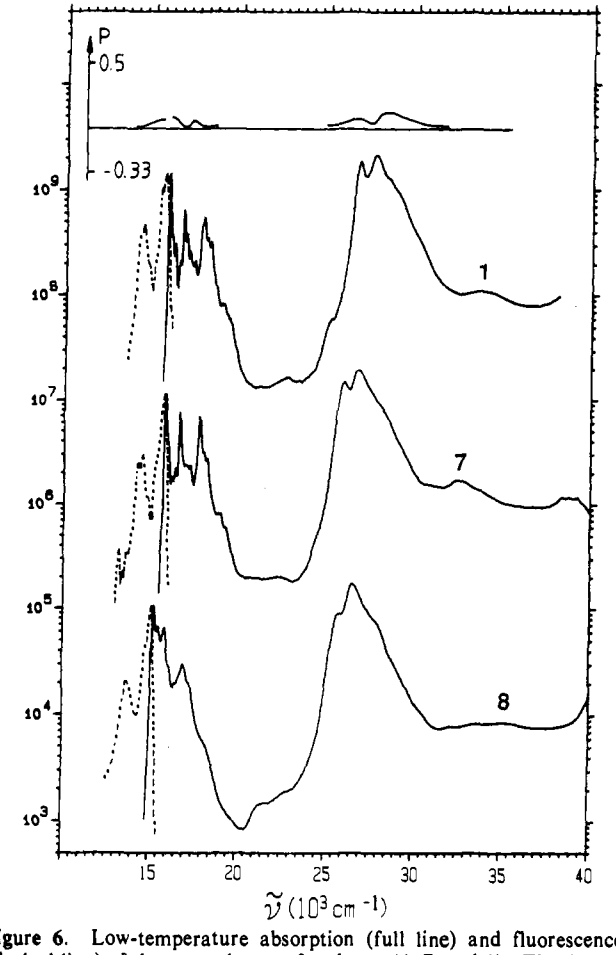

Figure 6. Low-temperature absorption (full line) and fluorescence (dashed line) of three porphycene free bases (**1**, **7**, and **8**). The degree of fluorescence polarization *P* is shown for **1** (fluorescence excited at 26 500 cm^{-1}, monitored at 15 700 cm^{-1}): solvent, 2-MTHF (77 K). The scale refers to the bottom spectrum. The other two are shifted by two or four decades upward.

but the observed variations lie within the experimental error of about 0.05 (Figure 6).

Within the experimental error, LD measurements done on stretched polyethylene sheets also failed to reveal any differences in polarization for the four low-energy bands. In this case, an obvious interpretation is to argue that the shape of the molecule resembles a perfect disk too much to develop any preferential orientation with respect to the in-plane axes. This type of explanation is not possible for the result of the fluorescence excitation measurement, and it is likely that motion of the internal protons is involved (see Discussion section). At higher energies, the absorption spectrum of **1** is a little more structured than for the other compounds (compare Table II). A relatively sharp MCD minimum is observed at 42 000 cm^{-1}.

Adding *n*-propyl substituents to the heterocyclic rings (**7**) has only little influence on the electronic spectra (Figures 6 and 7, Tables I and II), as was also true for the protonated compound **5**. The intensities are somewhat higher compared to those of **1**, and the Soret bands as well as the band around 42 000 cm^{-1} are shifted slightly toward lower energies. Transition X is only seen as a weak shoulder at about 24 300 cm^{-1}. All other relevant features, including relative intensities and the magnitude of the *B* terms, are nearly the same for both compounds.

As expected from the observation made on **6**, *n*-propyl substituents at the ethylene bridges (**8**) again have a somewhat larger influence (Figures 6 and 8, Table I). Compared to those of **1**, both the Q and the Soret bands of **8** are shifted by about 1000 cm^{-1} to lower energies. From the MCD spectrum, it is obvious that the third and not the second maximum that is observed in the low-temperature absorption spectrum (Figure 6) corresponds to the origin of Q_2, yielding a split between the two Q transitions

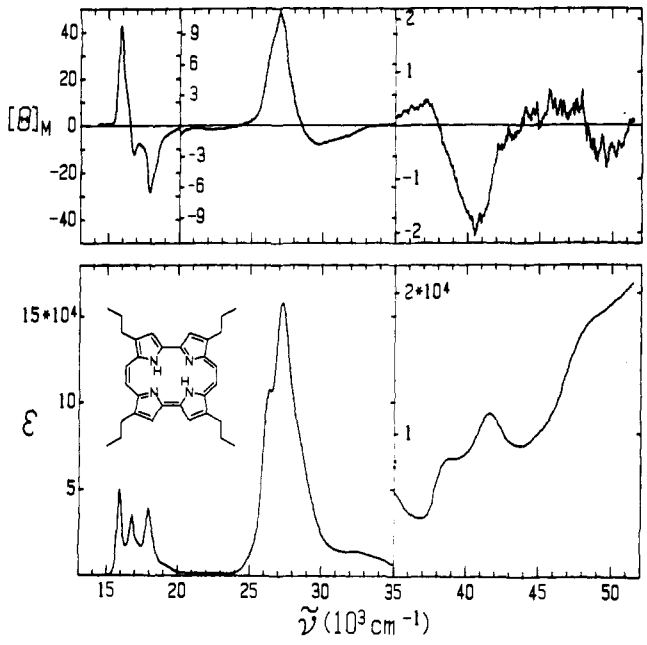

Figure 7. *n*-Propyl-substituted porphycene **7**: top, MCD; bottom, absorption; solvent, CH_3CN (room temperature).

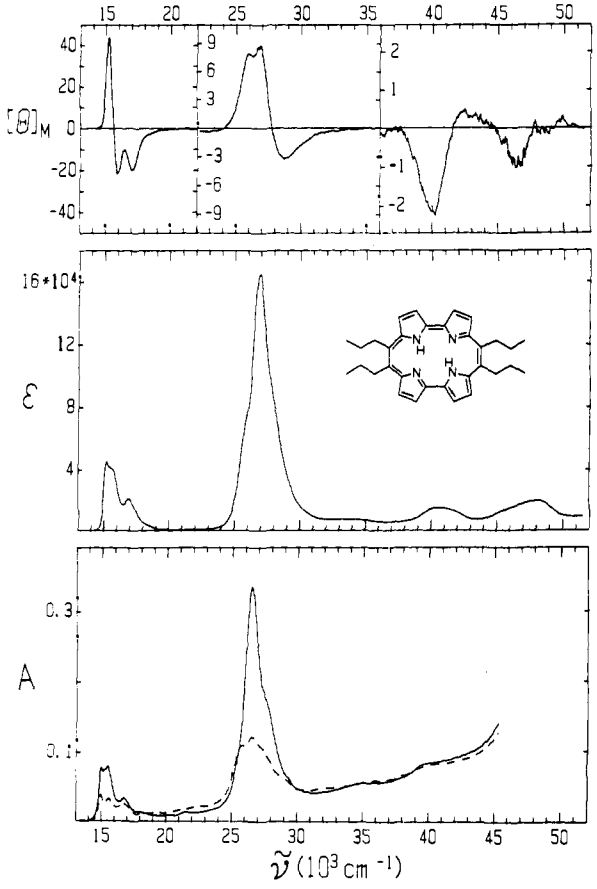

Figure 8. *n*-Propyl-substituted porphycene **8**: top, MCD; center, absorption; solvent, CH_3CN; bottom, absorption spectrum in stretched polyethylene sheets, full line indicates absorbance polarized parallel to the stretching direction and broken line indicates absorbance polarized perpendicular to the stretching direction; room temperature.

of about 600 cm^{-1}. The second absorption maximum results from a low-energy vibration of about 260 cm^{-1}. The above given assignment makes it quite likely that the situation is similar to that in **6**, thus putting the origin of Q_2 at 15 600 cm^{-1} for **8** (in 2-MTHF). At room temperature (Figure 8), the first Soret band appears merely as a shoulder on the low-energy side of the Soret-band region. As in **6**, it is resolved in the low-temperature

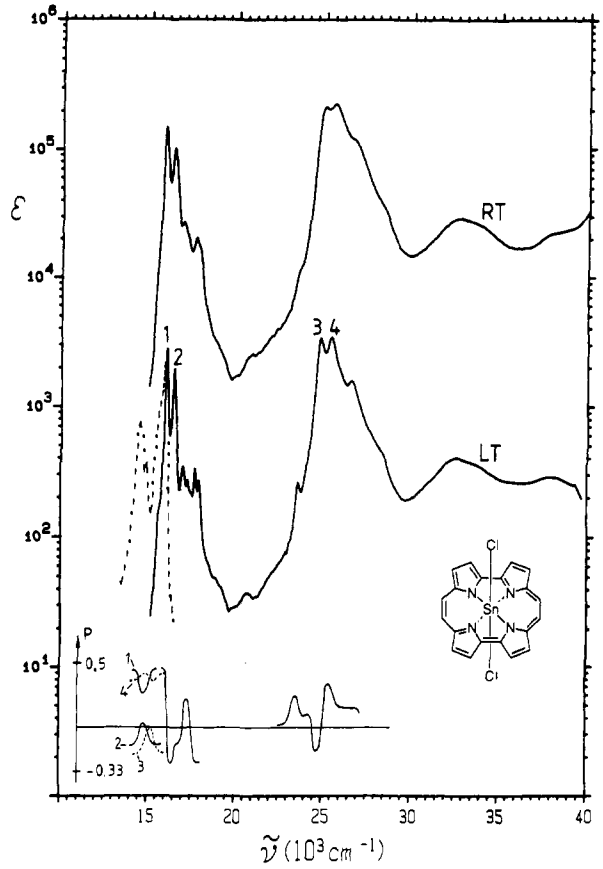

Figure 9. Porphycene $SnCl_2$ complex **9**: full line, absorption at room temperature (RT) and 77 K (LT); solvent, 2-MTHF; dashed line, fluorescence at 77 K; *P*, degree of polarization obtained from polarized fluorescence and polarized fluorescence excitation spectra. The numbers refer to the bands at which fluorescence was excited.

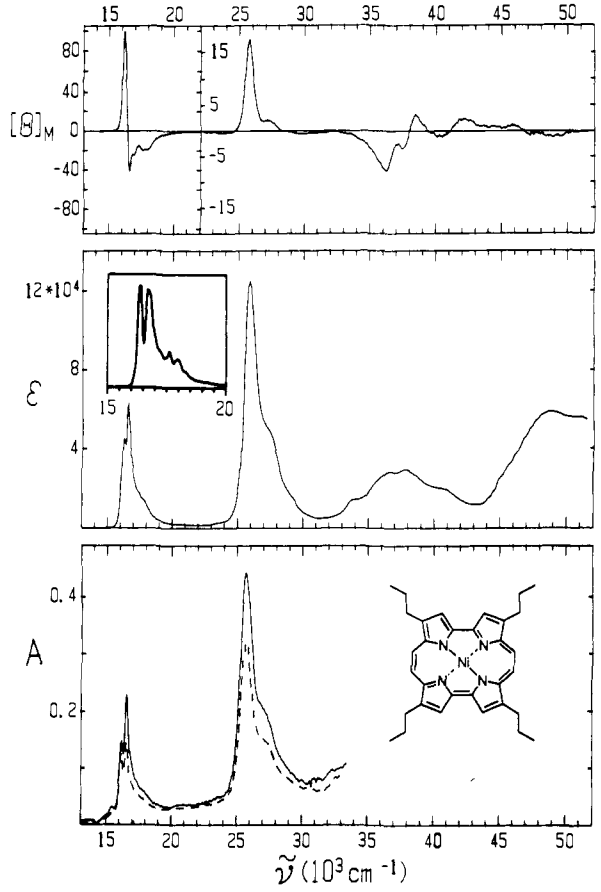

Figure 10. Porphycene Ni complex **10**. See caption to Figure 8. The inset shows the first band measured at 77 K.

spectrum (Figure 6). The band X is no longer seen in **8**, but some very weak absorption is now revealed between 21 500 and 24 000 cm^{-1}. This may be related to the shallow minimum in the MCD curve around 23 000 cm^{-1} that is seen in the free bases and in the metal salts. Neither type of *n*-propyl substitution, however, changes the MCD pattern observed in **1**, and in **7** as well as **8** both Soret bands have a negative *B* term. In both compounds, we observe again the MCD minimum that is attributed to an independent transition Y on the high-energy side of the Soret bands. Like **6**, the free base **8** with its pronounced long axis was well-suited for measurement of LD in stretched sheets (Figure 8). The lower-energy Soret band has a larger transition moment component in the direction of the short axis, the higher-energy Soret band along the long axis. For the Q bands, the result is not as clear but there is at least some indication that Q_1 is more nearly long-axis- and Q_2 more nearly short-axis-polarized.

Metal Salts. In all four metal salts investigated (**9–12**), the Q bands are about one order of magnitude more intense than the Q bands in **3**. The split between Q_1 and Q_2 is only about 500 cm^{-1} or less. Due to the strong overlap of the two Q bands the oscillator strengths for the individual transitions that are shown in Table I have to be considered only as rough estimates. The Soret bands now lie very close together and are split at most by a few hundred wavenumbers (Table I). At the low-energy onset of the Soret region (21 000–25 000 cm^{-1}), the weak band X that was not observed in **3–6**, and was only weakly indicated in **7**, is clearly visible in all three metal complexes.

The $SnCl_2$ complex of the parent porphycene **9** exhibits a strong fluorescence that allowed the measurement of well-resolved polarized emission and polarized excitation spectra. The degree of polarization is positive for the maximum at 15 920 cm^{-1} and negative for the maximum at 16 420 cm^{-1} (Figure 9). These two maxima are assigned to the origins of Q_1 and Q_2, respectively. Following these origins, we observe well-resolved vibrations of 1280 and 1260 cm^{-1} that have the same polarization as the origins of Q_1 and Q_2, respectively. In spite of the near degeneracy of the two Q bands, there is no indication of dual fluorescence. A vibrational frequency of about 350 cm^{-1} is seen in the fluorescence and also as a hot band in absorption.

In the Soret-band region, we observe two oppositely polarized bands, separated by only 600 cm^{-1}. The band at lower energy is polarized parallel to Q_2, leading to a polarization sequence ∥, ⊥, ⊥, ∥ for the four fundamental low-energy transitions. The band X observed at the low-energy side of the Soret region is polarized parallel to Q_1. At higher energies, the spectrum contains only bands with medium intensity and little structure (Table II). The fluorescence was not strong enough to allow us to measure the degree of polarization in this region.

In the nickel complex **10**, the origins of the two Q bands are only separated by about 300 cm^{-1} (Figure 10). In spite of the strong overlap that certainly leads to some cancellation of positive and negative contributions, **10** shows the largest *B* terms for the Q transitions among the porphycenes for which we measured MCD spectra. At 77 K, some vibrational structure is revealed in the Q-band region (inset in Figure 10). A low-energy vibration of about 260 cm^{-1} is indicated as shoulders following the Q_2 origin.

The two Soret bands have now fused into one single band (Figure 10), and it is no longer possible to estimate the splitting between them. The MCD curve also shows one single band in the Soret region that closely follows the shape of the absorption band. The *B* terms are both negative and much smaller in magnitude than the *B* terms of the Q bands (Table I).

In stretched polyethylene, the separation between Q_1 and Q_2 is somewhat increased (~400 cm^{-1}). The higher dichroic ratio (1.6) observed for the second part of the Q band (16 400–18 000 cm^{-1}) as compared to the dichroic ratio observed at the onset (1.1) shows that Q_2 is polarized parallel to the orientation axis. However, the location of this axis in the molecular frame is not known with certainty. For the Soret band, the dichroic ratio is exactly the average of what is found for the two Q bands as one

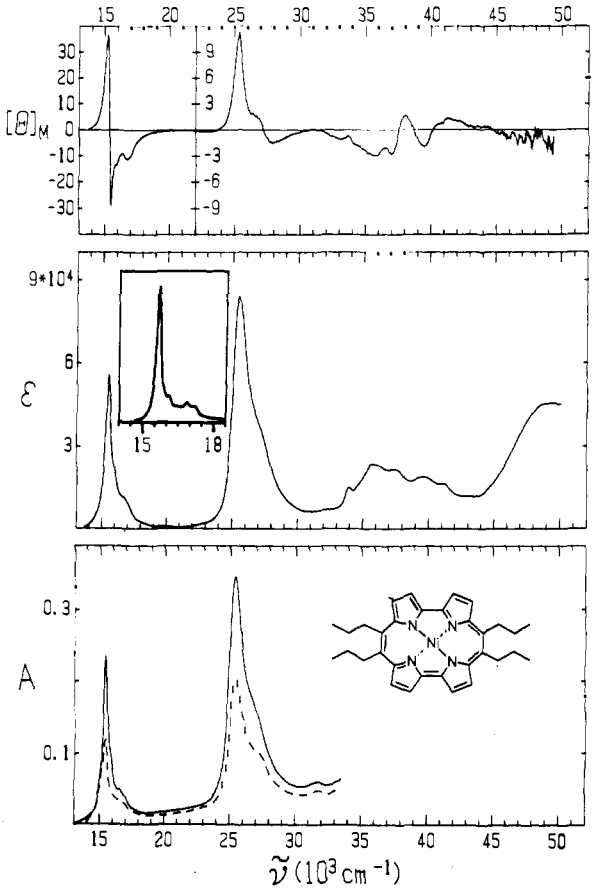

Figure 11. Porphycene Ni complex **11**. See caption to Figure 8. The inset shows the first band measured at 77 K.

would expect for two overlapping oppositely polarized transitions of comparable intensity.

A very small minimum, indicating a positive *B* term, is seen in the MCD curve in the range of the weak transition X. This transition is clearly seen as a shoulder in the 77 K absorption spectrum. Another MCD minimum is observed at the high-energy side of the Soret bands, indicating transition Y. At higher energies, a band of medium intensity is observed between 32 000 and 43 000 cm^{-1}. From the MCD curve, it is obvious that the shoulders in this band relate at least in part to different transitions (Table II). The same is certainly true for the second medium-intensity band that stretches from 43 000 to over 50 000 cm^{-1}.

In the isomeric nickel complex **11**, the four *n*-propyl groups are attached to the carbon atoms of the ethylene bridges. The molecule now has a pronounced long axis that should lead to a reasonable orientation in stretched polymer sheets. The Q bands are shifted by about 800 cm^{-1} toward lower energy compared to those of **10** (Figure 11). In the room-temperature absorption spectrum, the two Q bands are as indistinguishable as the two Soret bands. Even at 77 K, where we observe some vibronic fine structure in the Q-band region (compare inset in Figure 11), we are not able to separate the two origins and they are certainly closer than 300 cm^{-1}. The first MCD maximum at 15 250 cm^{-1} falls into the onset of the Q band. The first MCD minimum nearly coincides with the band maximum at 15 510 cm^{-1}. The dichroic ratio observed in stretched polyethylene (Figure 11) is smaller (1.2) in the region of the band onset than it is near the band maximum (1.8). In spite of the strong overlap of the two Q bands, this observation clearly indicates short-axis (y) polarization for Q_1 and long-axis (x) polarization for Q_2. The Soret bands are shifted by about 500 cm^{-1} compared to those of **10**. The dichroic ratio is nearly constant (1.6) in the whole Soret-band region, confirming the near degeneracy of the two Soret transitions. The X band, only seen as a shoulder at room temperature, becomes clearly visible at 77 K. Compared to that of **10**, the band is shifted similarly as the Q and the Soret bands. The MCD minimum at

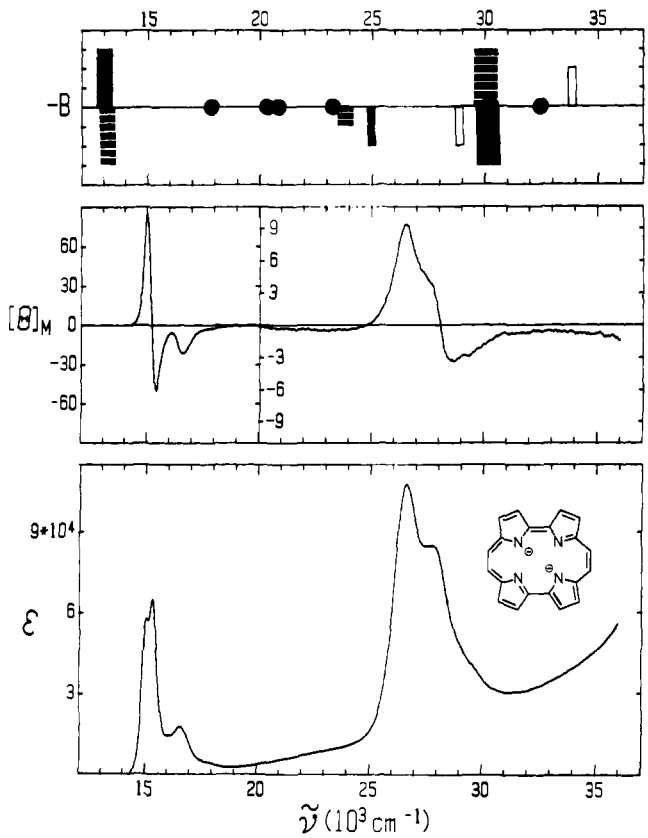

Figure 12. Porphycene dianion (**12**). See caption to Figure 1.

28 000 cm^{-1} that we assign to the Y band is somewhat more pronounced in **11** than in **10**. The rest of the spectrum is similar for **10** and **11**.

The spectra of the dipotassium salt **12** of parent porphycene **1** are similar to those of **10**. The Q bands are split detectably, by about 300 cm^{-1} (Figure 12). The intensity of the Q bands relative to that of the Soret bands is similar to what we found for the free bases **1**, **7**, and **8**. Removal of the two pyridine-type hydrogens does not increase the perturbation of the perimeter by the bridges very much. The strongest perturbations are encountered in the complexes **9**, **10**, and **11**.

Relative to those of the free base **1**, the Q bands of the dipotassium salt **12** are shifted to slightly lower energies, Q_1 by about 1000 cm^{-1}, and Q_2 by about 1600 cm^{-1}. The MCD intensity in the Q region is somewhat higher than in **11**, perhaps because of a smaller degree of cancellation, that in the Soret region is comparable. As in **10** and **11**, the two Soret transitions seem to be almost degenerate. Between 20 000 and 25 000 cm^{-1}, where we observe a shallow MCD minimum in all investigated compounds, a somewhat stronger absorption is observed for **12** ($f \simeq 0.15$) than for the other compounds. The Y transition is clearly indicated by the MCD minimum at 28 500 cm^{-1} and a corresponding shoulder in the absorption spectrum.

Discussion

The salient features of the spectra of porphycenes described in the preceding section are accounted for by CNDO/S, INDO/S, and PPP calculations, and can be understood semiquantitatively even in terms of the simple perimeter model. In view of previous experience with these procedures, this is not surprising. The CNDO/S results are given in the tables, the INDO/S results are shown in the figures, and the PPP results are not being published. All three types of calculations yield very similar results for symmetry-allowed transitions. Due to the presence of doubly excited configurations in the CNDO/S calculations, some of the experimentally unobserved symmetry-forbidden transitions are predicted to lie between the Q and the Soret bands.

Two aspects of the results are noteworthy. First, the porphycenes provide an excellent illustration of the interplay of the

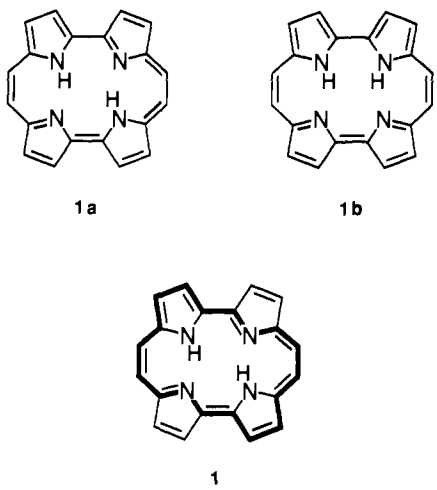

Figure 13. [18]Annulene-like conjugation path in porphycene (**1**).

so-called μ^+ and μ^- contributions[14] to the MCD spectra of perturbed annulenes, and this is discussed in detail in the following. Second, fluorescence polarization data for the free base **1** reveal the existence of interesting proton-transfer processes in the excited state. However, additional time-resolved experimental work is required before they can be fully elucidated.

The Perimeter as a Starting Point. Qualitative discussions of porphyrins and porphycenes have frequently involved the concept of an internal [18]annulene-like conjugation path embedded in the macrocycle[7a,24] (Figure 13). Such embedded paths can be formulated for all polycyclic π systems, but their formulation is particularly tempting in macrocycles consisting of a number of smaller, usually five-membered, rings connected by direct bonds or conjugating bridges to produce a macrocycle. Since the individual small rings offer cyclic conjugation in themselves, discussions of electronic structure have at times been cast in terms of competition between local cyclic interactions in the subunits and delocalization over the whole macrocycle and attempts were made to define the "main conjugation path".[24]

Since the choice of the internal conjugation paths is more or less arbitrary, they need to offer a clear-cut advantage over the otherwise natural choice of the outside perimeter as the starting point for the discussion of electronic properties. In **1** and **2**, reference is usually made to their aromatic stability and to the aromatic nature of [18]annulene.

For the understanding of electronic spectra and MCD of **1** and **2**, we believe it to be far preferable to start with the [20]annulene dication and to introduce four -NH- bridges as a perturbation leading to the doubly protonated dications of **1** or **2**. Alternatively, four $-N^-$- bridges lead to the dianions of **1** and **2**, and a combination of two -NH- with two $-N^-$- bridges leads to the neutral species **1** and **2**. One of the reasons for this choice is the fact that charged perimeters, such as the 18-π-electron [20]annulene dication, have a degenerate L_1, L_2 state pair, while neutral perimeters, such as [18]annulene, have a very large energy split between these two states. Since in **2**, and also in **1**, the two L states are almost degenerate, the electronic structure of these heterocycles exhibits more similarity with that of charged $(4N + 2)$-electron perimeters than with that of uncharged $(4N + 2)$-electron perimeters. In other words, the construction of **1** or **2** from [18]annulene by the bridging with two -NH- groups and two -CH=CH- groups and by two aza replacements represents a larger perturbation of the electronic states than their construction from [20]annulene dication by bridging with two -NH- and two $-N^-$- groups, and the latter thus represents a more suitable simple starting point for the analysis of electronic spectra.

The difference between **1** and **2** consists merely of different positions of attachment of the bridging -NH- and $-N^-$- groups (Figure 14). As might be suspected and as we shall indeed demonstrate below, this difference in topology dictates the differences in the electronic and MCD spectra of **1** and **2** in a transparent fashion. Comprehension will be facilitated if we first briefly review the use of the perimeter model for the derivation of MCD spectra.[14,25]

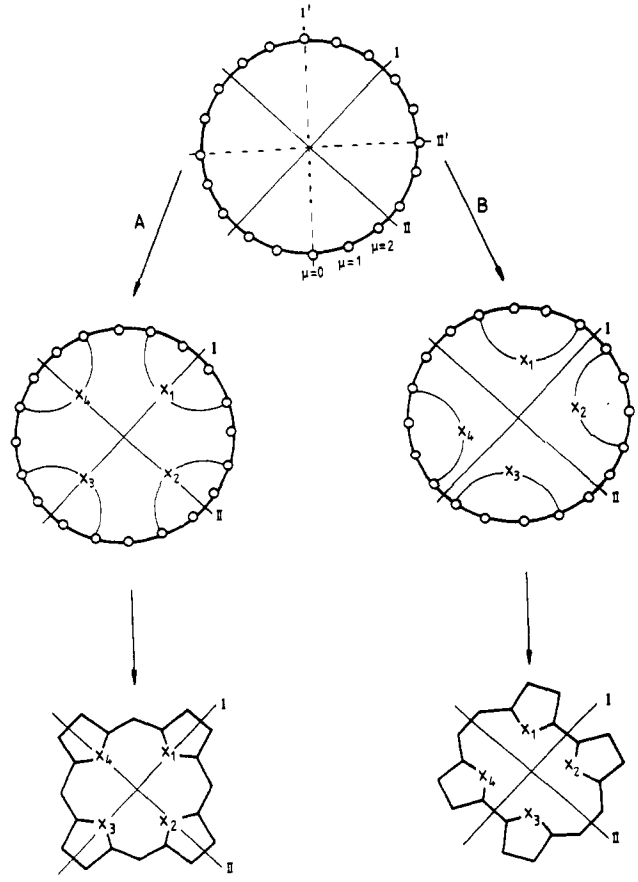

Figure 14. Development of chromophores of the porphyrin and porphycene types from a 20π-center perimeter.

The Perimeter Model for Porphyrins and Porphycenes.[11-14] As usual, the labeling of the $2p_z$ AO's along the perimeter in Figure 14 starts with $\mu = 0$. We introduce two sets of mutually orthogonal vertical mirror planes, one cutting through atoms, including the labeling origin $\mu = 0$ (I', II'), and the other through bonds (I, II). To derive a porphyrin-type system, the perturbing bridges have to be attached to atom pairs 1-4, 6-9, 11-14, and 16-19. The mirror planes I and II are preserved for $X_1 = X_3$ and $X_2 = X_4$ (D_{2h} porphyrins). For $X_1 = X_2 = X_3 = X_4$ (D_{4h} porphyrins), the mirror planes I' and II' are preserved, too.

To produce porphycenes, the bridges have to be attached to atom pairs 1-18, 4-7, 8-11, and 14-17. The mirror planes I and II are only preserved in those cases where all four X groups are equal (D_{2h} porphycenes). Congestion among internal hydrogens may cause out-of-plane distortions and symmetry reduction to approximate D_2. When $X_1 = X_2 \neq X_3 = X_4$, only the plane I is present (C_{2v} porphycenes), and when $X_1 = X_3 \neq X_2 = X_4$, mirror symmetry planes are absent (C_{2h} porphycenes).

Electronic States of a Charged $(4N + 2)$-Electron n-Atom Perimeter ($n \neq 4N + 2$). The molecular orbitals $|\psi_k\rangle$ (MO's) of the parent perimeter are symmetry-determined linear combinations of the n AO's $|\chi_\nu\rangle$ located on the n perimeter atoms. Their complex form is

$$|\psi_k\rangle = n^{-1/2} \sum_{\nu=0}^{n-1} \exp(2\pi i k\nu/n)|\chi_\nu\rangle$$

where $k = 0, \pm 1, \ldots \pm(n/2 - 1), n/2$ (n is even). Their energy increases with increasing $|k|$. In the ground configuration of the parent perimeter Ψ_G, the nondegenerate lowest energy MO $|\psi_0\rangle$ and all the degenerate levels up to the pair ψ_N, ψ_{-N} are doubly

(24) Gutman, I. *Croat. Chem. Acta* **1985**, *58*, 359.

(25) Michl, J. *Tetrahedron* **1984**, *40*, 3845.

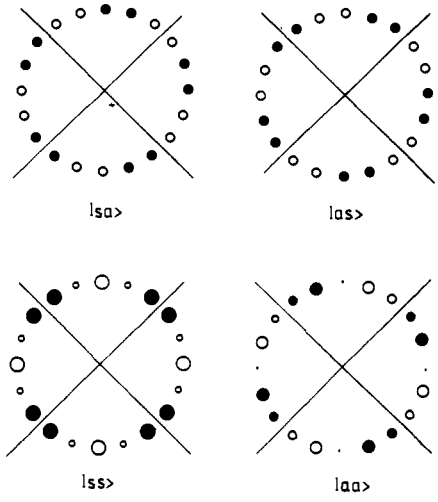

Figure 15. Two highest occupied ($|ss\rangle$ and $|aa\rangle$) and two lowest unoccupied ($|sa\rangle$ and $|as\rangle$) molecular orbitals of an unperturbed [20]annulene dication.

occupied. This configuration is taken to represent the ground state of the perimeter. The two components of the degenerate low-energy L state, which is of E_{2N+1} symmetry in the C_n group, are represented by the singly excited configurations $\Psi_N^{-N-1} \equiv |\psi_N\rangle \rightarrow |\psi_{-N-1}\rangle$ and $\Psi_{-N}^{N+1} \equiv |\psi_{-N}\rangle \rightarrow |\psi_{N+1}\rangle$. The two components of the degenerate higher energy B state, which is of E_1 symmetry, are represented by the singly excited configurations $\Psi_N^{N+1} \equiv |\psi_N\rangle \rightarrow |\psi_{N+1}\rangle$ and $\Psi_{-N}^{-N-1} \equiv |\psi_{-N}\rangle \rightarrow |\psi_{-N-1}\rangle$. Explicit algebraic expressions can be written for the transition intensities and MCD A and B terms of the [n]annulene perimeter.[14a,b] All the intensity is carried by the transition to the B state, and the L transition would have none in the absence of vibronic perturbations.

Electronic States of a Perturbed Charged ($4N + 2$)-Electron n-Atom Perimeter. For our purposes, the properties of a structural perturbation are adequately described by its one-electron part $\hat{A} = \sum_{j=1}^{4N+2} \hat{a}_j$, as described by its complex matrix elements a and b in the CI matrix written in the basis of the above configurations built from the complex MO's $|\psi_k\rangle$.[14] These are simultaneously the matrix elements for the mixing of the degenerate frontier orbitals by the perturbation:

$$a = |a| \exp(i \arg a) = \langle \Psi_{-N}^{N+1} | \hat{A} | \Psi_N^{N+1} \rangle = -\langle \psi_N | \hat{a} | \psi_{-N} \rangle$$

$$b = |b| \exp(i \arg b) = \langle \Psi_N^{-N-1} | \hat{A} | \Psi_N^{N+1} \rangle = \langle \psi_{-N-1} | \hat{a} | \psi_{N+1} \rangle$$

The perturbation converts the complex HOMO and LUMO pairs into real orbital pairs that no longer need to be degenerate. Their general appearance in the case of D_{2h} porphycenes is shown in Figure 15. The two highest occupied MO's $|ss\rangle$ and $|aa\rangle$ have four nodal planes perpendicular to the plane of the molecule. The two lowest unoccupied MO's $|sa\rangle$ and $|as\rangle$ have five such planes.

The complex parameters a and b that describe the structural perturbation have a simple physical interpretation. This is particularly transparent for their absolute value. To first order in degenerate perturbation theory, the energy difference of the now split HOMO pair is given by

$$\Delta\text{HOMO} = 2|a|$$

and that of the now split LUMO pair by

$$\Delta\text{LUMO} = 2|b|$$

The complex arguments of a and b, arg a and arg b, respectively, reflect the symmetry of the perturbation and dictate the position of nodes in the four resulting real orbitals.

From the orbital diagrams of Figure 15, it is obvious that a porphyrin-type perturbation cannot lift the degeneracy of the LUMO pair as long as all four perturbers X are equal. If the occupied atomic p_z orbital of the bridging atom has a lower energy than those of the perimeter atoms, the orbital labeled $|ss\rangle$ is pushed upward and we expect it to lie above $|aa\rangle$ by an amount dictated

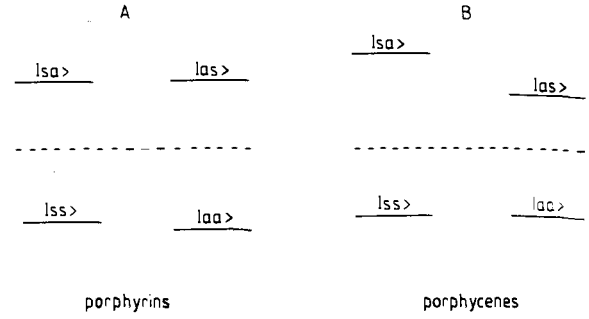

Figure 16. Splitting of the originally degenerate HOMO and LUMO pairs in a perturbed charged 18-electron 20-atom perimeter ($C_{20}H_{20}^{++}$).

by the strength of the C–X interaction, as determined by the resonance integral β_{CX} and by the ionization potential of the lone pair on X. Since the bridges are attached very close to the nodal points of $|ss\rangle$, the shift is small. As discussed earlier,[14a] the strength of the perturbation of the parent perimeter increases in the order X = –O– < X = –NH– < X = –N⁻–. This standard situation is depicted in Figure 16A.

Note that, here and elsewhere, we use the term "bridge" in the sense usual in the perimeter model, i.e., as a moiety with one (or more) orbitals of π symmetry attached to two (or more) atoms of the parent perimeter, such as the central nitrogen atoms in **1** or **2**. In porphyrin chemistry, the term bridge could also refer to an entity linking individual pyrrole rings, but this is not the sense in which we use it here.

For a porphycene-type perturbation, the order of perturbation strength is the same (–O– < –NH– < –N⁻–, i.e., **3** < **4**–**6** < **9**–**12**) but the topology and therefore the resulting situation are quite different. Now, the energy of the orbital $|as\rangle$ remains unperturbed to first order, whereas $|sa\rangle$ is perturbed strongly and shifted to higher energy. For the two HOMO orbitals, the effect of the perturbation is expected to be quite similar and they should remain "accidentally" nearly degenerate. This is borne out by numerical calculations. According to our CNDO/S calculations, in **3** and **4** $|aa\rangle$ lies a little (~0.15 eV) below $|ss\rangle$, whereas in **9** and **12** it lies above it by an even smaller amount (the metal in **9** was modeled by Be^{2+} in the calculation). This is probably a result of interplay between inductive and mesomeric effects of the bridge, the former dominating in **3** and **4** and the latter in **9** and **12**. At the INDO/S level of calculation, $|aa\rangle$ lies a little below $|ss\rangle$ in **3**, **4**, and **12** but in the case of **12** the difference is minuscule (0.005 eV).

The resulting level diagram is shown schematically in Figure 16B. The pattern of the splitting is very different for porphyrins (ΔHOMO small, ΔLUMO small or zero) and porphycenes (ΔHOMO small, ΔLUMO large), and we shall see below that this difference accounts immediately for the spectroscopic properties of porphycenes as contrasted with porphyrins.

It has been shown[14] that the effect of the one-electron perturbation $\hat{A}$ on the final states of the perturbed perimeter can be expressed algebraically. The eigenstates of the Hamiltonian for the perturbed perimeter can be thought of as mixtures of the components of the original degenerate perimeter states L and B. Except for the strongest perturbations, the resulting four states can still be identified in the order of increasing energy as originating from the original L_1, L_2, B_1, and B_2 states, respectively, and can be allowed to keep their labels.

The parameters α and β that describe the mixing of the components of the B state with those of the L state of the parent perimeter are simple functions of ΔHOMO and ΔLUMO:

$$\tan 2\alpha = 2(|a| + |b|)/[E(\text{B}) - E(\text{L})]$$

$$\tan 2\beta = 2(|a| - |b|)/[E(\text{B}) - E(\text{L})]$$

where $E(\text{B}) - E(\text{L})$ is the energy separation of the L and B states in the parent perimeter.

Dipole Strengths and Polarizations of Transitions in a Perturbed Charged ($4N + 2$)-Electron n-Atom Perimeter. Since the perturbed L states contain an admixture of the original B states of

the perimeter, they generally carry oscillator strength and possess nonvanishing B terms in MCD spectra.

Explicit expressions for transition dipole strengths D are

$$D(B_2) = 2m^2(n,2N + 1) \cos^2 \alpha$$

$$D(B_1) = 2m^2(n,2N + 1) \cos^2 \beta$$

$$D(L_2) = 2m^2(n,2N + 1) \sin^2 \beta$$

$$D(L_1) = 2m^2(n,2N + 1) \sin^2 \alpha$$

For relatively weak perturbations, we can set $\tan x = x$. We can then approximately relate α and β, and thus the dipole strengths, directly to ΔHOMO and ΔLUMO:

$$\alpha \simeq (\Delta\text{HOMO} + \Delta\text{LUMO})/2[E(B) - E(L)]$$

$$\beta \simeq (\Delta\text{HOMO} - \Delta\text{LUMO})/2[E(B) - E(L)]$$

For weak perturbations, it is also reasonable to replace the energy difference $E(B) - E(L)$ between the B and L states of the parent perimeter by the experimentally accessible energy difference between the average energy of the B states and the average energy of the L states of the perturbed perimeter. Thus, a separate measurement of the four dipole strengths permits the determination of the absolute values of the sum and difference of ΔHOMO and ΔLUMO. Note, however, that the sign of ΔHOMO $-$ ΔLUMO cannot be determined in this way.

The transitions to L_1 and B_2 are polarized along a direction $\mathbf{e}_1'$, obtained by defining a vector $\mathbf{e}_1$ pointing from the center of the parent perimeter to atom number 0 and rotating it counterclockwise by angle $\gamma = (\arg a + \arg b)/2$ around the vector $\mathbf{e}_3$, located in the out-of-plane C_n axis. Transitions into L_2 and B_1 are polarized along $\mathbf{e}_2'$, perpendicular to both $\mathbf{e}_1'$ and $\mathbf{e}_3$. The polarization directions relative to L_1 therefore are $\parallel (L_1)$, $\perp (L_2)$, $\perp (B_1)$, $\parallel (B_2)$. The values of the angles arg a and arg b, which determine the absolute polarization directions, follow from their definitions.[14b] In order to find arg a, one inspects the location of the nodal points in the more stable of the two MO's derived from the degenerate perimeter HOMO, relative to their location in a real perimeter HOMO chosen to have a nodal point at the atom $\mu = 0$. If the nodes in the perturbed MO are displaced in the clockwise direction by h bond lengths, arg $a = (4Nh + n)\pi/n$. In order to find arg b, one examines the nodal properties of the more stable of the two MO's derived from the degenerate perimeter LUMO in the same fashion, except that the number (l) of bond lengths by which the nodes of the perturbed orbital have been displaced relative to a real perimeter LUMO with a nodal point at the atom $\mu = 0$ is measured counterclockwise, and arg $b = 4\pi(N + 1)l/n$.

The situation is simple in the molecules of D_{2h} symmetry **3**, **4**, **9**, and **12** (Figures 14–16), in which the nodal properties of the MO's are easily deduced by inspection. Since the orbital $|as\rangle$ always lies below $|sa\rangle$, its nodal properties determine arg b. With the atom numbering used in Figure 14, we have $l = 1.5$ by inspection of Figure 15 and thus arg $b = -\pi/2$. If the orbital $|aa\rangle$ lies below $|ss\rangle$, as CNDO/S predicts for the more weakly perturbed porphycenes **3** and **4** and as INDO/S predicts for **3**, **4**, and **12**, the nodal properties of the orbital $|aa\rangle$ are used to find arg a. By inspection of Figure 15, $h = 0$ and thus arg $a = \pi$. If the orbital $|aa\rangle$ lies above $|ss\rangle$, as CNDO/S predicts for the more strongly perturbed porphycenes **9** and **12**, the nodal properties of the latter are to be used. Then, $h = 1.25$ and thus arg $a = 0$. The angle γ therefore equals $\pi/4$ if $|aa\rangle$ lies below $|ss\rangle$, as expected from CNDO/S for **3** and **4** and from INDO/S for **3**, **4**, and **12**. It equals $-\pi/4$ if $|aa\rangle$ lies above $|ss\rangle$, as expected from CNDO/S for **9** and **12**. Using these simple arguments based on orbital energies alone, in the first two molecules (**3**, **4**), the transitions to L_1 and B_2 are thus expected to be polarized along the long (x) axis and transitions to L_2 and B_1 along the short (y) axis, regardless of whether CNDO/S or INDO/S is used to derive the orbital sequence. According to INDO/S, **12** should behave the same way. However, according to CNDO/S, the MO sequence in **12** is such that L_1 and B_2 should be y-polarized and L_2 and B_1 x-polarized in **9** and **12**. These are indeed exactly the polarizations obtained from numerical CI calculations by the two methods.

The polarization directions can be understood simply in terms of configuration or orbital energy differences: When $|aa\rangle$ lies below $|ss\rangle$, the lowest excited singlet is dominated by the configuration $|ss\rangle \rightarrow |as\rangle$; when $|aa\rangle$ lies above $|ss\rangle$, the lowest excited singlet is dominated by the configuration $|aa\rangle \rightarrow |as\rangle$, and polarization directions follow from state symmetries. The close relation between orbital energies and configuration energies is a consequence of the properties of the unperturbed perimeter orbitals. For these, configuration energy differences are equal exactly to orbital energy differences. The CNDO/S and INDO/S MO's of the porphycenes are sufficiently similar to the unperturbed perimeter orbitals that configuration and orbital energy differences can still be used interchangeably for a nearly degenerate pair.

The quantity $m(n,2N + 1)$ is a simple geometrical function of n, N, and perimeter bond length.[14a] Strictly speaking, the formulas for dipole strength only apply to a regular polygon perimeter. Upon distortion of the perimeter geometry, different values of $m(n,2N + 1)$ should be used for differently polarized transitions. An elongation along the $\mathbf{e}_1'$ direction with a simultaneous flattening along the $\mathbf{e}_2'$ axis will increase the value appropriate for $D(B_2)$ and $D(L_1)$ and reduce the value appropriate for $D(B_1)$ and $D(L_2)$. For molecules under consideration presently, these effects are relatively small and will be ignored in the following.

***B* Terms of Transitions in a Low-Symmetry Perturbed Charged (4*N* + 2)-Electron *n*-Atom Perimeter.** For perimeters perturbed in such a way that no rotation axes of symmetry higher than C_2 are present, A terms in the MCD spectra are absent and the B terms are

$$B(B_2)/D(B_2) = \mu^-(n,N)\{\cos^2 \beta[E(B_2) - E(B_1)]^{-1} + \sin^2 \beta[E(B_2) - E(L_2)]^{-1}\} + \mu^+(n,N)(\sin 2\alpha \sin 2\beta/4 \cos^2 \alpha) \times \{[E(B_2) - E(B_1)]^{-1} - [E(B_2) - E(L_2)]^{-1}\}$$

$$B(B_1)/D(B_1) = \mu^-(n,N)\{-\cos^2 \alpha[E(B_2) - E(B_1)]^{-1} + \sin^2 \alpha[E(B_1) - E(L_1)]^{-1}\} - \mu^+(n,N)(\sin 2\alpha \sin 2\beta/4 \cos^2 \beta) \times \{[E(B_2) - E(B_1)]^{-1} + [E(B_1) - E(L_1)]^{-1}\}$$

$$B(L_2)/D(L_2) = \mu^-(n,N)\{-\cos^2 \alpha[E(B_2) - E(L_2)]^{-1} + \sin^2 \alpha[E(L_2) - E(L_1)]^{-1}\} + \mu^+(n,N)(\sin 2\alpha \sin 2\beta/4 \sin^2 \beta) \times \{[E(B_2) - E(L_2)]^{-1} + [E(L_2) - E(L_1)]^{-1}\}$$

$$B(L_1)/D(L_1) = -\mu^-(n,N)\{\cos^2 \beta[E(B_1) - E(L_1)]^{-1} + \sin^2 \beta[E(L_2) - E(L_1)]^{-1}\} + \mu^+(n,N)(\sin 2\alpha \sin 2\beta/4 \sin^2 \alpha) \times \{[E(B_1) - E(L_1)]^{-1} - [E(L_2) - E(L_1)]^{-1}\}$$

The relative energies of the states of the perturbed perimeter, $E(L_1)$, $E(L_2)$, $E(B_1)$, and $E(B_2)$, assumed here to be nondegenerate, along with the already familiar CI mixing parameters α and β, thus determine the multiplication coefficients at the magnetic moments $\mu^+(n,N)$ and $\mu^-(n,N)$ that compose each of the B terms. The magnetic moment $\mu^+(n,N)$ is negative and about an order of magnitude larger than the moment $\mu^-(n,N)$.[14a] The latter is also negative, except for the case of highly negatively charged parent perimeters, which is not of interest presently.

The physical interpretation of the μ^+ contribution and of the μ^- contribution to a B term has been discussed.[14,25] We shall see below that porphycenes provide a very nice example of their interplay.

Like the dipole strengths D, the μ^- contributions to the B terms depend only on the magnitude but not the sign of α and β, i.e., on the sum of ΔHOMO and ΔLUMO and on the absolute value of their difference $|\Delta\text{HOMO} - \Delta\text{LUMO}|$. Only the magnitudes of the μ^- contribution, but not their signs, are structure-sensitive.

In contrast, the signs as well as the magnitudes of the μ^+ contributions to the B terms are determined by the factor $\sin 2\alpha \sin 2\beta$ and are responsible for the unique structural sensitivity of the MCD method for perimeter-derived systems. While α is always positive, β is positive only when $\Delta\text{HOMO} > \Delta\text{LUMO}$ and negative when $\Delta\text{HOMO} < \Delta\text{LUMO}$. In the case $\Delta\text{HOMO} = \Delta\text{LUMO}$, the μ^+ contributions vanish. Chromophores in which this special situation occurs are referred to as "soft" since minor

structural perturbations can then induce one or the other signs for ΔHOMO − ΔLUMO and thus for the μ^+ contributions to their B terms and for the observed MCD signs.[14] The free-base porphyrin chromophore nearly satisfies this condition in that its ΔHOMO − ΔLUMO value is positive but quite small, and minor substitution effects are indeed capable of dictating its MCD signs.[5b,14b,23]

Chromophores in which ΔHOMO − ΔLUMO is large are likely to keep its sign, and therefore the signs in their MCD spectra, even after significant structural perturbation. They are referred to as "hard": positive-hard if ΔHOMO > ΔLUMO and negative-hard if ΔHOMO < ΔLUMO. The μ^+ contributions to the spectra of positive-hard and of negative-hard MCD chromophores are mirror images of each other.[14]

Since in π systems derived from charged perimeters both the energy gap ΔL between the two L states and the gap ΔB between the two B states are typically much smaller than the L–B energy separation, we have

$$[E(B_2) - E(B_1)]^{-1}, [E(L_2) - E(L_1)]^{-1} \gg [E(B_2) - E(L_2)]^{-1}, [E(B_1) - E(L_1)]^{-1}$$

and it is a reasonable first approximation to consider only the terms resulting from the B_2–B_1 and L_2–L_1 magnetic mixing in analyzing the MCD spectra. Then, one obtains

$$B(B_2) = -B(B_1) = (m^2/2\Delta B)(4\mu^- \cos^2\alpha \cos^2\beta + \mu^+ \sin 2\alpha \sin 2\beta)$$

$$B(L_2) = -B(L_1) = (m^2/2\Delta L)(4\mu^- \sin^2\alpha \sin^2\beta + \mu^+ \sin 2\alpha \sin 2\beta)$$

Remembering that both μ^+ and the much smaller μ^- are negative, the consequences of this simple result for the MCD signs are straightforward. For relatively weak perturbations, α and β are small, and as long as ΔL and ΔB are comparable the μ^- contribution to the B terms is much larger for the B bands than for the L bands, where it can usually be neglected altogether. The signs of the contributions provided by the μ^- term are positive for L_1 and B_1 and negative for L_2 and B_2, regardless of the nature of the structural perturbation of the perimeter. Under the same conditions, the μ^+ contributions to the B terms of both the L bands and the B bands are similar. In positive-hard chromophores ($\beta > 0$), their signs agree with those of the μ^- contributions and there is no doubt about the outcome: The predicted B term sign sequence is +, −, +, − in the order of increasing energy, regardless of the overall strength of the perturbation that converted the parent perimeter into the system under consideration.

In contrast, in negative-hard chromophores ($\beta < 0$), the signs of the μ^+ contributions to the four B terms are exactly opposite to those of the μ^- contributions. Now, as the strength of the perturbation of the parent perimeter increases, the μ^+ contribution will dominate $B(L_1)$ and $B(L_2)$, which will be negative and positive, respectively, but it will initially not be able to dominate $B(B_1)$ and $B(B_2)$, whose μ^- contribution is nonvanishing from the outset. With increasing strength of the perturbation, the simple theory thus leads one to expect a gradual sign reversal, from $B(B_1) > 0$, $B(B_2) < 0$ in the parent perimeter and weakly perturbed derivatives (α, β small) to $B(B_1) < 0$, $B(B_2) > 0$ for very strongly perturbed perimeters (α, β large). In the present approximation, both $B(B_1)$ and $B(B_2)$ should vanish when the μ^- and μ^+ contributions just cancel, i.e., for

$$\tan\alpha \tan\beta = -(\mu^-/\mu^+) \qquad \beta < 0$$

Note that this can be rewritten as

$$\frac{\sqrt{D(L_1)D(L_2)}}{\sqrt{D(B_1)D(B_2)}} = \frac{\mu^-}{\mu^+}$$

and this relation holds even for perimeters distorted from the shape of an ideal polygon. Often, however, strong overlap makes the separate determination of the four dipole strengths difficult. As long as the dipole strengths of the two members of each set of transitions (L and B) do not differ excessively ($\alpha \simeq \beta$), geometric mean can be replaced by arithmetic mean, so that the condition becomes

$$\frac{D(L_1) + D(L_2)}{D(B_1) + D(B_2)} = \frac{D(L)}{D(B)} = \frac{\mu^-}{\mu^+}$$

Approximating tan x by x as before, this condition can also be rewritten as

$$\Delta HOMO^2 - \Delta LUMO^2 = -4(\mu^-/\mu^+)[E(B) - E(L)]^2$$

For the $C_{20}H_{20}^{++}$ perimeter, μ^-/μ^+ has been estimated[14a] at about 0.1. Therefore, for porphycenes with $D(L)/D(B)$ values less than about 0.1, the signs of the B terms of the Soret bands, $B(B_1)$ and $B(B_2)$, should be dictated by the μ^- contribution and the overall sign sequence should be −, +, +, −. For large values of $D(L)/D(B)$, these signs should be dictated by the μ^+ contribution and the overall sign sequence should be −, +, −, + in the order of increasing energy.

The strength of perturbation required to reach the crossover point is relatively difficult to attain in practice, and it is common for the MCD signs of the L bands to be dictated by the μ^+ contribution, while those of the B bands are dictated by the μ^- contributions. The latter are therefore generally much less useful for structural applications. We shall see below that porphycenes represent a rare example of a system in which the strength of the perturbation of a perimeter can be raised in a nearly continuous fashion to produce a negative-hard chromophore in which the condition for mutual cancellation of the μ^+ and μ^- contributions to the B terms of the B bands has been almost met.

However, in order to understand the predicted behavior of B terms in the vicinity of the critical point and in order to understand the differences in the absolute magnitudes of $B(L_1)$ and $B(L_2)$ and of $B(B_1)$ and $B(B_2)$, we need to return to the full formulas for the B terms without neglecting $[E(B_2) - E(L_2)]^{-1}$ and $[E(B_1) - E(L_1)]^{-1}$. These make it clear that the mutual magnetic mixing of the L and the B states, whose effect has been ignored until now, will reinforce the μ^+ contributions to $B(L_2)$ and $B(B_1)$ and reduce those to $B(L_1)$ and $B(B_2)$. The opposite is true for the μ^- contribution. Since μ^+ and μ^- contributions have opposite signs in negative-hard chromophores, the inclusion of the so far ignored L–B magnetic mixing terms has two interesting consequences: (i) the magnitude of the B term of L_2 should always exceed that of L_1 and (ii) the expected change of the sign of the B terms of the B bands with increasing strength of perturbation should first happen for B_1. Here both terms that result from the L–B magnetic mixing have the same sign as the μ^+ contribution. For B_2, they have the same sign as the μ^- contribution. Thus, we expect that there will be a range in the perturbation strength for which both B bands have negative B terms.

Porphycene. Spectral Interpretations. The identification of the Q and Soret regions, respectively, with the L and B transition pairs expected from the perimeter model is straightforward. The expected order of increasing strength of perturbation of the parent $C_{20}H_{20}^{++}$ perimeter, –O– < –NH– < –N⁻–, is reflected well in the dipole strength ratio $D(L)/D(B)$, which increases steadily in the order **3 < 4–6 < 9–12** (Table I), presumably reflecting the growing size of ΔHOMO − ΔLUMO (Tables III–VIII).

As long as the two Q and the two Soret bands overlap pairwise so strongly that it is not possible to derive their individual dipole strengths, $D(L)/D(B)$ is the best experimental measure for the overall strength of the perturbation. The expected order of increasing perturbation strength is also reflected well in the behavior of the B terms: The B term of the Q_1 band becomes increasingly more negative and that of the Q_2 band more positive. At the same time, the initially quite strongly positive B term of the lower Soret band gradually decreases, changes sign, and then becomes distinctly negative and the originally strongly negative B term of the upper Soret band approaches zero.

For the *tetraoxa compound* **3**, the $D(L)/D(B)$ ratio is only 0.066. It is then not surprising that this compound shows the smallest absolute values for the B terms of the Q bands, a fact that cannot be explained solely as a result of the somewhat larger

Table III. CNDO/S Results for Tetraoxaporphycene Dication (**3**)[a]

	E^b	f^c	polarizn[d]	$\delta_{\uparrow\uparrow}{}^e$	Ω^f
1	15010 L_1 (Q_1)	0.0003	x		
2	15400 L_2 (Q_2)	0.005	y		
3	28280		z	3.4	1.50
4	30300			5.6	1.04
5	30710		z	551.3	1.50
6	30840			34.5	1.23
7	32320 B_1	1.81	y		
8	32720			3.0	0.62
9	33030 B_2	2.38	x		
16[g]	42080	0.11	x		
29[g]	51250	0.38	y		

[a] ΔLUMO = 0.2430 eV, ΔHOMO = 0.1409 eV, and $D(L)/D(B)$ = 0.0025. [b] Transition energy (cm^{-1}), including ground-state depression. [c] Oscillator strength (dipole length). [d] Polarization. [e] Two-photon absorption cross-section for two equally linearly polarized photons (10^{-50} cm^4 s $photon^{-1}$ $molecule^{-1}$). [f] Two-photon polarization parameter.[27] [g] Transitions with $f > 0.1$.

Table IV. CNDO/S Results for N-Protonated Porphycene Dication (**4**)[a,b]

	E	f	polarizn	$\delta_{\uparrow\uparrow}$	Ω
1	15240 L_1 (Q_1)	0.058	x	0.011	1.50
2	15500 L_2 (Q_2)	0.028	y	0.006	1.50
3	24430		z	3.2	1.50
4	27160			59.3	0.69
5	29040		z	14.4	1.50
6	29360			462.1	1.13
7	29840			53.6	1.32
8	31450 B_1	1.29	y	0.04	1.50
9	32570 B_2	1.70	x	0.07	1.50
11[c]	36180		x		
20[c]	41250		x		
22[c]	44600		x		
24[c]	45470		y		

[a] See footnotes to Table III. [b] ΔLUMO = 1.0307 eV, ΔHOMO = 0.1662 eV, and $D(L)/D(B)$ = 0.060. [c] Transitions with $f > 0.1$.

difference between their energies ΔQ (compare **1**, **4**, and **7**).

The result of the CNDO/S calculation confirms the weakly perturbing character of the oxygen bridges (Table III). ΔLUMO is only slightly larger than ΔHOMO, a situation typical for a soft chromophore. The frontier orbitals are very close to the ideal perimeter orbitals, and the Q and Soret transitions result nearly exclusively from the four HOMO → LUMO excitations. In spite of the fact that the relative energies are predicted reasonably well, the perturbation is underestimated in the CNDO/S calculation. The calculated oscillator strengths for the Q bands, and therefore also the calculated $D(L)/D(B)$ ratio, are much too small. The sequence of polarization direction predicted for the four low-lying one-photon allowed transitions is x, y, y, x. The same sequence is found in the INDO/S result (Figure 1) and also from the perimeter model, once the calculated orbital sequence $|aa\rangle$ below $|ss\rangle$ is accepted. The predicted sign sequence for the B terms is −, +, +, −, as one would expect for a nearly soft (only weakly negative-hard) chromophore. The calculation also predicts B terms of similar magnitude for the Q and the Soret bands, in accordance with the experimental findings. The failure of the MCD minimum to coincide with the absorption maximum at 26200 cm^{-1} is most likely due to the strong overlap of the two Soret bands. It is, however, not possible to rule out an influence of higher excited states, the magnetic coupling with which is not included in the simple model. Since **3** is a nearly soft chromophore (ΔHOMO $\simeq$ ΔLUMO), these contributions could be of some importance for the B terms of the Soret bands.

Due to the difficulties in the interpretation of polarization data, we cannot directly confirm the sequence of the Q and Soret bands predicted by the calculations. There is, however, a hint that the calculated order is correct at least for the Q transitions. A force field calculation (QCFF/PI[26]) predicts frequencies of 101 and 341 cm^{-1} for the two lowest a_g vibrations. The lower frequency corresponds to a vibration in which the upper and the lower half of the molecule in formula **3** oscillate against each other along y and the higher frequency to a vibration in which the left and the right part of the molecule oscillate against each other along x. Since the lower frequency couples more strongly to Q_2 and the higher frequency more strongly to Q_1, it is perhaps likely that these transitions are indeed polarized along y and x, respectively.

Four additional transitions are calculated between the Q and the Soret bands at the CNDO/S level. The transitions are one-photon electric-dipole forbidden as long as the molecule has a center of symmetry. All four transitions are predicted to be two-photon-active, but due to the very low energy of the Q transitions, it is most likely impossible to search for these transitions by monitoring the two-photon absorption via fluorescence.[27] The only possibility seems to be the application of the thermal blooming method.[28] In agreement with the experimental results, the calculations do not predict further transitions with an oscillator strength higher than 0.1 up to 50000 cm^{-1}.

The second lowest relative Q-band intensity is found for the *protonated porphycenes* **4**, **5**, *and* **6**. For all three compounds, $D(L)/D(B)$ lies between 0.16 and 0.21 (Table I), a value somewhat higher than the 0.1 estimated for the turning point from weak to strong perturbation in the B terms of the Soret bands. Unfortunately, we do not have an X-ray structure for these compounds. It is, however, obvious that they are no longer planar. In order to obtain a reasonable input geometry for the CNDO/S calculation, we used the following procedure: We first constructed a symmetrized planar structure from the known X-ray data for porphycene free base[6] by averaging the atomic positions. We shall refer to this as the idealized D_{2h} geometry. We then tilted the heterocyclic rings so as to make the distance between the central hydrogen atoms equal to twice the van der Waals radius. The resulting D_2 geometry was similar to that obtained from a QCFF/PI force field calculation. The twist angles in the perimeter system that resulted from this procedure were on the order of 25–30°. The result of the CNDO/S calculation is shown in Table IV. ΔHOMO is small, as expected for all porphycene-type perturbations, but ΔLUMO is now considerably larger than ΔHOMO, confirming that the protonated species are undoubtedly negative-hard chromophores. The intensity of the Q bands is still underestimated, but not as much as in the case of **3**. The calculated value for $D(L)/D(B)$ is 0.051. Even though the separation of the Soret bands is largest in the protonated species, it is not possible to compare the calculated and experimental oscillator strengths of the individual transitions because of the still quite strong overlap in the two band systems. The calculation predicts the same sequence of polarization directions as for **3**, as does the perimeter model as long as $|aa\rangle$ lies below $|ss\rangle$, but no experimental information on these is available. The Q and Soret transitions still contain between 75% (upper Soret) and 90% (Q_1) of the HOMO → LUMO excitations.

The INDO/S calculation (Figure 3) predicts a sign sequence of −, +, −, −. This is the sequence we expect from the perimeter model for the transition region between weak and strong perimeter perturbation. However, it is obvious from the experiment that we are still in the weak perturbation regime, albeit closer to the intermediate case. In spite of the fact that the gaps between the components of the Q and the Soret bands are similar, the B terms of the Soret bands are now an order of magnitude smaller than those of the Q bands. As expected from our general considerations, the Q_2 and the upper Soret band in **4**, **5**, and **6** again have the larger absolute B term within each pair.

As in the case of **3**, neither CNDO/S nor INDO/S predicts a transition between Q_2 and the Soret bands that is one-photon-allowed. A transition of medium intensity is predicted about 4000 cm^{-1} above the Soret band. We assign this transition to the spectral feature labeled Y that we observe in the MCD spectrum of **4** and in the absorption spectrum of **6**.

(26) Warshel, A.; Karplus, M. *J. Am. Chem. Soc.* **1972**, *94*, 5612. Lifson, S.; Warshel, A. *J. Chem. Phys.* **1968**, *49*, 5116.

(27) Hohlneicher, G.; Dick, B. *Pure Appl. Chem.* **1983**, *55*, 261.

(28) Twarowski, A. J.; Kliger, D. S. *Chem. Phys.* **1977**, *20*, 253, 259.

Table V. CNDO/S Results for the trans Tautomer of Porphycene Free Base (**1a**)[a]

	D_{2h} geometry[b,d]				QCFF/PI geometry[e]		
	E	f	Φ[c]		E	f	Φ[c]
1	14810 L_1 (Q_1)	0.056	−51.4	1	13990 L_1 (Q_1)	0.038	−59.4
2	17540 L_2 (Q_2)	0.113	45.1	2	16750 L_2 (Q_2)	0.124	69.6
3	25910			3	23350		
4	26650			4	24630		
5	27320 X	0.095	−38.2	5	26110 X	0.105	−26.8
6	29680			6	28260		
7	31040			7	30160		
8	31620			8	31030 B_1	0.87	69.9
9	31830			9	31330		
10	32080 B_1	1.01	63.9	10	32180		
12[f]	33370			12[f]	33780 B_2	1.32	−15.0
14[f]	34930 B_2	1.50	−22.1	17[f]	34370	0.37	−13.7
19[f]	39960 Y	0.30	49.0	22[f]	39950 Y	0.54	49.6
23[f]	40930	0.17		24[f]	42190	0.11	
24[f]	41590	0.23		28[f]	43530	0.23	
27[f]	43980	0.28		34[f]	48370	0.32	
29[f]	46370	0.09					

[a] See footnotes to Table III. [b] A C_{2h} geometry derived from the idealized D_{2h} geometry by adding the internal protons (see text). [c] The angle between the transition moment and the horizontal axis of formula **1**, measured counterclockwise. [d] ΔLUMO = 1.2636 eV, ΔHOMO = 0.1435 eV, and $D(L)/D(B)$ = 0.14. [e] ΔLUMO = 1.2037 eV, ΔHOMO = 0.4195 eV, and $D(L)/D(B)$ = 0.15. [f] Transitions with $f > 0.1$.

Table VI. CNDO/S Results for the cis Tautomer of Porphycene Free Base (**1b**)[a]

	"D_{2h} geometry"[b,d]				QCFF/PI geometry[e]		
	E	f	polarizn		E	f	polarizn
1	15540 L_1 (Q_1)	0.059	y	1	19280	0.131	y[c]
2	17720 L_2 (Q_2)	0.068	x	2	20650	0.035	x
3	24960	0.009	y	3	26820	0.123	x
4	26360	0.060	x	4	27650	0.016	y[c]
5	27360	0.001	x	5	29910	0.013	y[c]
6	28980	0.435	y	6	32060	0.54	y[c]
7	29210	0.001	z	7	32770	0.001	x
8	30580	0.142	y	8	33380	0.86	x
9	32280			9	34780	0.35	x
10	32600	0.044	x	10	35350	0.049	y[c]
11	32790	0.016	y	11	36440	0.025	x
12	33000	0.027	x	12	38410	0.11	y[c]
13	33540	0.81	x	13	39150	0.17	x
14	35960	0.38	y	15[f]	41050	0.09	x
16[f]	37470	0.49	x	18[f]	43320	0.11	x
19[f]	39230	0.10	y	23[f]	45090	0.22	y[c]
29[f]	46050	0.24	x	27[f]	46990	0.13	y[c]
31[f]	46800	0.11	x				

[a] See footnotes to Table III. [b] A C_{2h} geometry derived from the idealized D_{2h} geometry by adding the internal protons (see text). [c] The transition moment deviates somewhat from the y direction since the molecule is not fully planar. [d] ΔLUMO = 1.1063 eV, ΔHOMO = 0.0190 eV. [e] ΔLUMO = 1.1519 eV, ΔHOMO = 0.5419 eV. [f] Transitions with $f > 0.1$.

Table VII. CNDO/S Results for the Beryllium Complex of Porphycene (**1**)[a,b]

	E	f	polarizn	$\delta_{\uparrow\uparrow}$	Ω
1	16200 L_1 (Q_1)	0.103	y		
2	16680 L_2 (Q_2)	0.094	x		
3	26410			7.2	1.50
4	27980			29.8	1.43
5	30520			233.9	1.47
6	31280			4.4	1.50
7	31520 X	0.20	y		
8	31880			69.3	1.50
9	32550 B_1	0.88	x		
10	32970			4267.0	0.25
11	33320			6270.8	1.50
14[c]	34490 B_2	0.97	y		
16[c]	38260 Y	0.51	x		
18[c]	40790	0.25	x		
24[c]	44360	0.25	x		

[a] See footnotes to Table III. [b] ΔLUMO = 1.4059 eV, ΔHOMO = 0.0735 eV, and $D(L)/D(B)$ = 0.22. [c] Transitions with $f > 0.1$.

Table VIII. CNDO/S Results for Porphycene Dianion (**12**)[a,b]

	E	f	polarizn	$\delta_{\uparrow\uparrow}$	Ω
1	14740 L_1 (Q_1)	0.147	y		
2	15660 L_2 (Q_2)	0.184	x		
3	20410			16.5	1.47
4	21330			8.1	1.50
5	23740			68.1	0.26
6	26510			1.2	1.50
7	26760	0.018	y		
8	28630	0.039	x		
9	28910			150.0	1.50
10	28990			4440.3	1.38
11	29460			19382.4	1.50
12	29860				
13	32820 B_1	0.25	x		
15[c]	34060 B_2	1.21	y		
20[c]	38600 Y	0.50	x		
24[c]	40560	0.18	y		
33[c]	44500	0.33	x		
41[c]	47410	0.15	y		
42[c]	47420	0.44	x		
47[c]	49410	0.17	y		

[a] See footnotes to Table III. [b] ΔLUMO = 2.1704 eV, ΔHOMO = 0.0170 eV, and $D(L)/D(B)$ = 0.50. [c] Transitions with $f > 0.1$.

For the *free bases* **1**, **7**, *and* **8**, the ratio $D(L)/D(B)$ is about twice larger than for the protonated porphycenes **4–6**, indicating a considerably stronger perturbation of the parent perimeter. This agrees with the fact that we no longer observe a positive MCD band in the Soret region. The perturbation now has reached a strength where the B term of the lower Soret band is close to zero or even negative. This is in accordance with the expectations we

derived from the perimeter model.

When we try to compare our experimental findings for the porphycene free bases with more quantitative calculations, we face some problems due to possible tautomeric equilibria. In spite of the fact that X-ray structures are known for the porphycenes **1**, **7**, and **8**,[6,7] we do not know exactly which geometry to use for our calculations. The observed structures are close to D_{2h}, with the two internal hydrogens distributed nearly equally among the four possible positions. The problem is complicated by the fact that, for solutions, we cannot exclude the presence of the cis tautomer **1b** in addition to the more commonly assumed **1a**. From NMR studies,[8b] it appears that **1a** dominates but that the cis form is present to some extent at room temperature. This is quite different from porphyrin **2** where the cis form is only considered as a transient within the proton transfer process that converts one trans form into the other.[29]

If proton transfer in porphycene free base is as rapid in the solid state as it is in solution,[8b] the observed X-ray structure is a weighted average of the two possible trans structures **1a** (t and t') and of the two possible cis structures **1b** (c and c'). If, due to the influence of an asymmetric crystal field, the proton transfer is frozen in the solid state, the two tautomers t and t', and possibly also c and c', may still be present in approximate 1:1 ratios. It is not possible to decide between these two possibilities from the experimental information available at present.

For our present purpose, both explanations cause the same problem. The structure that is derived from the X-ray analysis is not the structure of a single tautomer relevant on the time scale of an electronic transition.

To shed some light on the problem, we performed force field calculations (QCFF/PI) for the cis and trans forms of porphycene free base **1**. The resulting geometries are shown in Figure 17 together with the statically or dynamically averaged geometry from the X-ray analysis. For the trans form, QCFF/PI predicts a larger difference between the two different heterocyclic rings than found in the X-ray geometry. The rings with pyridine-type nitrogens show pronounced bond lengths alternation for the C–C bonds. For the bonds outside the heterocyclic rings, the force field calculation predicts aromatic bond lengths with little bond length alternation, in good agreement with the observed X-ray structure. For the cis form, the situation is quite different and now it is possible to draw a single mesomeric structure. The QCFF/PI result closely resembles that structure. Only the bonds in the pyrrole rings are "aromatic", and all other parts of the molecule show strong bond length alternation. The trans and cis forms are calculated to be of comparable stability, with the cis form predicted to be 7.7 kcal/mol more stable than the trans form. For a system of this size, such a value certainly lies within the error limits of QCFF/PI.

In order to find out how changes in geometry may influence the electronic spectra of free-base porphycene tautomers **1a** and **1b**, we performed CNDO/S calculations for two geometries: (i) a geometry derived from the "idealized D_{2h} geometry" mentioned earlier by adding the internal protons (the N–H bond lengths were 1.000 Å) and (ii) the geometry obtained from the QCFF/PI calculation.

The results for the C_{2h} trans form are shown in Table V. In spite of the fact that the differences between the two different heterocyclic rings are fairly pronounced in the QCFF/PI geometry, calculations for the two geometries yield very similar results. Even the most sensitive quantities, the transition dipole moment directions, differ by less than 15°. Both calculations predict an additional one-photon-allowed transition between the Q and Soret transitions, polarized approximately parallel to Q_1. It corresponds mainly to an excitation from one of the lower π orbitals into LUMO.

For the C_{2v} cis form, the results of the calculations for the two geometries are quite different (Table VI). For the delocalized "D_{2h} geometry", the result is similar to that found for the trans

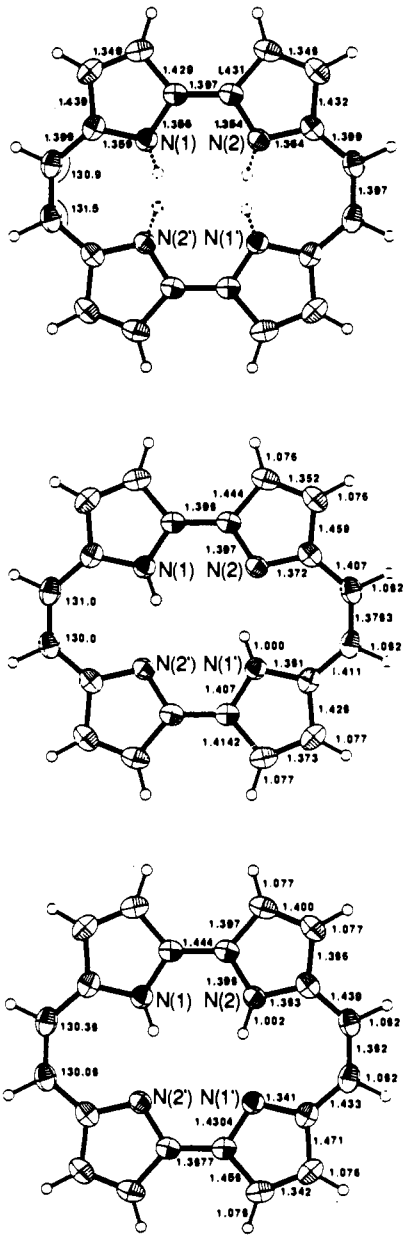

Figure 17. X-ray geometry of porphycene free base **1** (top) compared to the results of QCFF/PI calculations for the trans (center) and cis (bottom) tautomers.

form. The predicted energies of the Q transitions are nearly identical in the two cases. In the Soret region, we now find four instead of two strongly allowed transitions, but they are so close together that it will be difficult to distinguish them experimentally. The same is most likely true for the predicted differences in the polarization sequence. For the strongly localized QCFF/PI geometry, the calculation predicts a shift of the Q transitions by about 5000 cm^{-1} toward higher energies and the disappearance of a characteristic Soret band.

From the above results, it is difficult to tell whether the cis form contributes to the observed spectra of **1**. Within the limits imposed by the different spectral resolution at different temperatures, we do not find an indication for a temperature-dependent equilibrium in the region of the Q bands. The MCD curve does not indicate the presence of two superimposed bands, either. From this, we can estimate an upper limit of 20% cis form if this form is reasonably well described by a delocalized geometry. If the real geometry is, however, close to the localized QCFF/PI geometry, we expect the Q bands to appear around 20000 cm^{-1}, where the absorption of the trans form has a minimum. Here we should see the cis form if its fraction exceeds 5%. It may well be that the weak absorptions seen in this region in **1**, **7**, and especially

(29) Schlabach, M.; Rumpel, H.; Limbach, H.-H. *Angew. Chem., Int. Ed. Engl.* **1989**, *28*, 76.

8, and clearly distinct from the shoulder attributed to transition X, are indeed due to the presence of the cis form. Taken together, the evidence suggests that it is very unlikely that, in the solvents we have used, the fraction of the cis form exceeds 20% in the ground state. More detailed studies are, however, necessary to narrow this margin further.

After ruling out a major contribution from the cis form, we can finally analyze our experimental findings on the basis of the calculations made for the trans form (Table V). Compared to protonated porphycene (**4**), both calculations predict a slightly larger ΔLUMO and about twice as large oscillator strengths for the Q transitions. This is in full accord with the expected increase in the strength of the perturbation. The additional allowed transition calculated between the Q and the Soret transitions is assigned to the band labeled X that is clearly observed in **1** and indicated as a shoulder in **7**.

The polarization sequence calculated by the CNDO/S and INDO/S methods for the first five allowed transitions in **1** is approximately ∥ (L_1), ⊥ (L_2), ∥ (X), ⊥ (B_1), ∥ (B_2), where the L_1 transition moment lies nearly exactly along the NH–NH direction. For the four Q and Soret transitions, this is the same relative sequence as in the symmetrical molecules **3**, **4**, and **12**, where the L_1 transition moment direction however lies along the x axis. Due to the depolarization observed in fluorescence excitation, we cannot prove this sequence experimentally in **1**. We only know that the lower Soret band of the substituted derivative **8** is polarized somewhat more in the direction of the short axis y and the upper one somewhat more in the direction of the long axis x. This agrees with the CNDO/S calculations (Table V) and qualitatively also with what has been observed for **3** and **4**.

The sign sequence of the B terms predicted for the free base **1** by the INDO/S calculation is −, +, −, +. This is the sequence expected from the perimeter model for very strong perturbations. The measured MCD spectrum clearly shows that the −, + limit for the two Soret bands is not reached, and INDO/S seems to overestimate the strength of the perturbation. Only a PPP calculation that included next-nearest-neighbor resonance integrals yielded the sign sequence −, +, −, − that agrees with our experimental findings. At higher energies, both calculations (CNDO/S and INDO/S) predict somewhat more intense transitions compared to those of **3** and **4**. This, too, is in agreement with the experimental data.

The metal salts **9–12** exhibit the highest value for the ratio $D(L)/D(B)$. We now approach a limit where the perturbation of the parent perimeter is quite severe. Unfortunately there are no generally accepted parameters for transition metals like Ni or Sn in CNDO/S. We therefore used a beryllium complex as a model for the experimentally investigated compounds. The input geometry was taken from the X-ray structure[30] of the Ni complex of unsubstituted **1** with the beryllium atom placed in the center of the molecule. The result of the calculation is shown in Table VII. ΔHOMO is still very small, less than 0.1 eV, but ΔLUMO is now 1.4 eV. The near degeneracy of the two Q and the two Soret transitions that we observed in the experimental spectra is indeed reflected in the CNDO/S result: The transitions are not only close in energy, but now they also have similar intensities. The calculated value for $D(L)/D(B)$ is 0.21, a factor of about 2 larger than for the free base **1**.

The CNDO/S-predicted polarization sequence now is y, x, x, y for Q_1, Q_2, and the two Soret bands, and agrees with expectations from the perimeter model for the orbital ordering $|aa\rangle$ above $|ss\rangle$. It is exactly the opposite from what we obtained for the dications **3** and **4**. As in porphycene free base, an additional allowed transition is predicted at the low-energy side of the Soret bands. This transition has the same polarization direction as Q_1. The new transition is again attributed to the feature labeled X in our experimental spectra (Table I). The predicted polarization sequence is in full agreement with the observed relative polarizations, but we do not know the absolute orientation of the transition moments from experiment. However, the fact that, in **9**, the additional transition X has the same polarization as Q_1 makes it very likely that these transitions are indeed y-polarized. This conclusion is further confirmed by the LD measurements on **11** where we observe short (y) axis polarization for Q_1 and long (x) axis polarization for Q_2. Since the same behavior is observed in the isomer **10**, we suggest that, also in this molecule, the orientation axis is directed along x in Chart I.

From the MCD spectra of **10** and **11** in the range of the Soret band, it is obvious that, in the Ni complexes, we are close to the situation where a sign sequence −, +, −, + is reached. The MCD in the high-energy member of the Soret transition pair is much smaller than before, and the B term of B_2 now approaches zero.

On the high-energy side of the Soret bands, several medium-intensity transitions are predicted in our model calculation. For all three complexes, the absorption spectrum between 30 000 and 50 000 cm^{-1} shows more intense bands than for the other compounds investigated. It is, however, obvious from the MCD spectra that these structures result from a number of different transitions.

The calculations for the *porphycene dianion* **12** were again based on the D_{2h} geometry derived from the X-ray data for **1**. The results are shown in Table VIII and Figure 12. As expected from our general considerations, the predicted perturbation is much stronger than in the other theoretically investigated compounds. ΔLUMO is still fairly small, but ΔHOMO is now 2.17 eV and the calculated value for $D(L)/D(B)$ reaches 0.48. This is more than twice the value obtained for the Be complex. It is remarkable that even such a strong perturbation does not shift the four main transitions by more than 2000 cm^{-1}. For the Q_1, Q_2, and the Soret transitions, CNDO/S calculations predict the polarization sequence y, x, x, y, respectively. This is the same sequence as obtained for the Be complex. The only experimental hint that this prediction might be correct comes from the fact that the 0–0 transition of Q_2 is now more intense than the 0–0 transition of Q_1, as calculated, unlike what was observed for **1–8**. The INDO/S result disagrees and yields the polarization sequence x, y, y, x for these four transitions. We consider this less likely to be correct, particularly in view of the y, x, x, y experimental result for **11**. As shown in Table VIII and Figure 12, both calculations predict two additional allowed transitions between Q_2 and the Soret bands, one polarized along x and one along y. These might relate to the somewhat stronger unstructured absorption observed between 20 000 and 25 000 cm^{-1}.

Clearly, a correct theoretical prediction of the order of the nearly degenerate Q bands is very difficult, and the fact that CNDO/S apparently gives the right answers is most likely a coincidence. Conversely, one may view the experimental determination of the order of the x- and y-polarized transitions as an exquisitely fine probe for a relative configuration (and orbital) energy differences that occur in approximate quantum mechanical models.

The predicted B term sequence (Figure 12) corresponds to the strong perturbation limit (−, +, −, +). This is not surprising, since INDO/S gave that result already for the free base **1** where the calculated value for $D(L)/D(B)$ was only half as large as in **12**. For the two additional transitions between Q_2 and the Soret bands, INDO/S predicts small positive B terms in agreement with the experimental observations.

As far as we can judge from the experimentally observed ratio $D(L)/D(B)$, **12** is not as strongly perturbed as the calculations predict. $D(L)/D(B)$ is not much larger than in the free bases **1**, **7**, and **8**, and the MCD pattern in the Soret band region is similar to what we observe for the free bases and the metal complexes. One obvious explanation for this difference between theoretical predictions and experimental observations is that we do not observe the free dianion. If the counterions are in close proximity, we have a situation that reflects more the situation encountered in a metal complex. There is even a possibility that the system deviates from planarity in order to allow a better contact between the nitrogen lone pairs and the potassium ion or ions.

Excited-State Proton Transfer in Free-Base Porphycene. We finally return to the peculiar observation that the degree of fluorescence polarization in the three investigated porphycene free bases **1**, **7**, and **8** is very low (0.1 ± 0.05) and nearly constant.

(30) Lex, J. Private communication.

Table IX. Expected Degrees of Polarization P with the Fluorescence of Porphycene Free Base (**1**) upon Excitation of Different Transitions for Different cis–trans Equilibria in the Ground and Excited States[a]

		g		
	e	1.0	0.5	0
L_1 $(Q_1)^b$	2.0	0.16	0.19	0.22
	0.5	0.19	0.28	0.37
	0	0.22	0.37	0.50
L_2 $(Q_2)^b$	1.0	0.15	0.11	0.06
	0.5	0.16	0.30	−0.12
	0	0.17	−0.06	−0.33
$B_1{}^b$	1.0	0.19	0.21	0.22
	0.5	0.29	0.33	0.37
	0	0.37	0.43	0.50
$B_2{}^b$	1.0	0.17	0.11	0.06
	0.5	0.01	−0.06	−0.12
	0	−0.17	−0.25	−0.33

[a] The values have been calculated from the transition moment directions listed on the left-hand sides of Tables V and VI. See text. [b] The transition excited.

For a single species, such a result is only possible if the transition moments of all absorbing transitions have an angle of about 50° with the moment of the emitting transition. Such a situation is intrinsically very unlikely. It is also in disagreement with the perimeter model and with the results of our calculations. For the lowest excited state, it would imply that the transition moment has to rotate by about 50° between absorption and emission. The possibility that the emission comes from a different silent state below Q_1 is very unlikely, too, because of the small Stokes shift and the pronounced similarity between the absorption and emission spectra.

A much more plausible explanation can be given when we remember the rapid proton transfer that was observed in the ground state.[8b] If the proton transfer within the two hydrogen bridges is rapid also in the excited state, we have to consider the possibility that the emission comes from either of the originally excited trans tautomers t or t′ produced by a double proton shift. The transition moment of Q_1 is expected from theory to be oriented nearly exactly along the NH–NH direction. If t is converted into t′ within the lifetime of the lowest excited state, the moment of the emitting transition is rotated by about 90° relative to that of the absorbing transition. If the proton transfer is rapid with respect to the lifetime of Q_1, the emission will come from t or t′ with equal probability. The angle between the absorbing and emitting moments will then be 0° for half of the molecules and about 90° for the other half. From the angles shown on the left-hand side of Table V, we obtain[18b,31] the following P values: $P(L_1) = 0.16$, $P(L_2) = 0.15$, $P(B_1) = 0.19$, and $P(B_2) = 0.17$. Rapid proton transfer in the excited state thus can easily account for nearly constant P values on the order of $^1/_7$, the value expected for transitions involving a degenerate electronic state.

The explanation suggested so far has a serious drawback in that it completely ignores the cis form. Although this does not dominate the ground state, its fraction most likely is not negligible, and for all we can tell, it may dominate the excited L_2 state entirely.

We next consider the presence of all four possible forms, t, t′, c, and c′. As a first assumption, we neglect possible site effects that may occur in the glass in which the measurements are made. With this assumption, t and t′ are energetically equivalent in both the ground and excited states, and so are c and c′. The probability of finding a given molecule as the trans tautomer is g in the ground and e in the excited state. The proton transfer is assumed to be rapid enough to establish full thermodynamic equilibrium before significant fluorescence occurs, and c and t are assumed to have absorption and emission spectra that are indistinguishable within the experimental resolution. The expected[18b,31] P values are shown in Table IX for selected values of the parameters g and e, using transition moment directions from the CNDO/S calculations performed for the D_{2h} geometries (Tables V and VI). Although the calculated angles are certainly not known with an accuracy better than ±15°, and although site effects have been ignored, the entries of Table IX are quite consistent with the experimental observations as long as the cis form is present in the ground state to an extent smaller than about 50% ($g \geq 0.5$) and as long as the trans form dominates the excited state ($e > 0.5$). Given the uncertainties in the calculated angles, even the case where the cis tautomer dominates the ground state ($g < 0.2$) and the trans tautomer dominates the excited state ($e > 0.8$) is compatible with the experimental findings. In this latter case, the emission should be shifted to the red with respect to absorption. The shift that is needed to fulfill the above discussed conditions is, however, only on the order of 250 cm^{-1} (an energy difference of 100 cm^{-1} leads to an equilibrium distribution of 0.13 to 0.87 at 77 K).

We conclude that the low and nearly constant P values observed in the fluorescence polarization of porphycene free bases are compatible with the assumption of an excited-state proton-transfer process that is fast with respect to the lifetime of the lowest excited state. A certain amount of cis form in the ground state is acceptable as long as this form is not dominant in the excited state.

Summary

Structural variation has remarkably little effect on the excitation energies of the principal transitions of porphycene, but it has a noticeable effect on relative band intensities and a striking effect on absolute band polarizations and particularly the MCD spectra, although the signs of the L bands remains unaffected. All the qualitative trends are very well accounted for by the perimeter model. The CNDO/S, INDO/S, and PPP methods provide semiquantitative agreement.

Along the series of gradually more strongly perturbing bridges –O– < –NH– < –N⁻–, the $C_{20}H_{20}{}^{++}$ perimeter is converted from a soft to a negative-hard MCD chromophore. Simultaneously, we expect a change from a –, +, +, – B term sequence to the limiting sequence –, +, –, + as a result of a delicate interplay of the μ^- and μ^+ contributions to the B terms of the Soret band. The latter sign pattern is not reached, but an intermediate case is. For this intermediate case, the sign sequence –, +, –, – is expected, and it should be reached when the dipole strength ratio $D(L)/D(B)$ reaches about 0.1. Experimentally, the turning point is only reached at significantly higher values, about 0.5. A further analysis of this discrepancy may help to develop better quantitative predictions not only for the signs of B terms but also for their absolute magnitude.

Acknowledgment. We express our gratitude to the NATO Office of Scientific Research for the support of this collaborative project. The authors at Texas acknowledge support from the U.S. National Science Foundation (Grant CHE9000292).

Note Added in Proof. An investigation of UV–visible and resonance Raman spectra of metal salts of 2,7,12,17-tetrapropylporphycene has just been published: Oertling, W. A.; Wu, W.; López-Garriga, J. J.; Kim, Y.; Chang, C. K. *J. Am. Chem. Soc.* **1991**, *113*, 127.

Registry No. 1a, 100572-96-1; **1a** Be complex, 133730-21-9; **1b**, 133730-20-8; **3**, 113088-08-7; **4**, 133730-14-0; **5**, 133730-15-1; **6**, 133730-16-2; **7**, 133730-17-3; **8**, 133752-58-6; **9**, 133730-19-5; **10**, 110096-34-9; **11**, 127713-80-8; **12**, 133730-18-4.

(31) Czekalla, J.; Liptay, W.; Döllefeld, E. *Ber. Bunsen-Ges. Phys. Chem.* **1964**, *68*, 80.